Universidade de Aveiro

2021

PEDRO BATALHA GUINCHO

BIOTINTAS INOVADORAS BASEADAS EM PECTINA E NANOCELULOSE PARA APLICAÇÃO EM BIO-IMPRESSÃO 3D

NOVEL PECTIN AND NANOCELLULOSE BASED BIOINKS FOR 3D BIOPRINTING APPLICATIONS

Universidade de Aveiro
2021

PEDRO BATALHA GUINCHO

BIOTINTAS INOVADORAS BASEADAS EM PECTINA E NANOCELULOSE PARA APLICAÇÃO EM BIO-IMPRESSÃO 3D

NOVEL PECTIN AND NANOCELLULOSE BASED BIOINKS FOR 3D BIOPRINTING APPLICATIONS

Dissertação apresentada à Universidade de Aveiro para cumprimento dos requisitos necessários à obtenção do grau de Mestre em Bioquímica, especialização Clínica, realizada sob a orientação científica da Doutora Carmen Sofia da Rocha Freire, Investigadora Principal do Departamento de Química da Universidade de Aveiro e co-orientação do Doutor Nuno Hélder da Cruz Simões Silva, investigador Doutorado do CICECO/ Departamento de Química da Universidade de Aveiro.

This work was financially supported by the project "I&D NANOBIOINKS- Engineering bio-based nanofibers for the development of high-performance nanostructured bioinks for 3-D bioprinting, CENTRO-01-0145- FEDER-031289- funded by the Operational Program of the Center Region, in its FEDER/FNR component, and by national funds (OE), through FCT/MCTES.

Dedico este trabalho aos meus pais, a eles devo tudo o que sou e serei.

o júri

presidente

Prof. Doutor Brian James Goodfellow
Professor Associado do Departamento de Química da Universidade de Aveiro

Doutor Gil Alberto Batista Gonçalves
Investigador do Centro de Tecnologia Mecânica e Automação da Universidade de Aveiro

Doutora Carmen Sofia da Rocha Freire Barros
Investigadora Principal do Departamento de Química da Universidade de Aveiro

agradecimentos

Desejo agradecer à Doutora Carmen Freire e ao Doutor Nuno Silva pelo apoio incondicional que prestaram em todos os momentos desta dissertação. Um muito obrigado por acreditarem em mim e por me ajudarem a fazer desta dissertação algo real.

A todos os colegas de laboratório que me ajudaram sempre que precisei.

Aos meus amigos de Aveiro, que ajudaram a tornar esta viagem académica um dos melhores momentos da minha vida.

Aos meus amigos da Nazaré, António, Alexandre, Marcos, Francisco e Rui, que me acompanham desde sempre e espero que para sempre.

Agradeço de coração cheio à minha namorada Beatriz, que mesmo nos piores momentos, me deu luz e força para continuar.

Agradeço a toda a minha família os que estão e os que já não estão, todos os momentos que passei com eles e todos os ensinamentos que me deram e que contribuíram para estar hoje aqui a escrever este texto.

Agradeço ao meu irmão Ricardo, podemos ter as nossas disputas, mas sei que estará sempre lá para me apoiar quando for preciso. Adoro-te mano.

Por último, agradeço aos meus pais Carlos e Herondina por me darem a oportunidade de estudar, de sempre me darem espaço e possibilidades de ser o que eu quisesse, de me guiarem com os “Junta-te aos maus e serás como eles, junta-te aos bons e serás melhor que eles” e por todo o amor. Obrigado do fundo do coração, sou eternamente grato por tudo o que fizeram e fazem por mim.

Obrigado!

palavras-chave

Bio-impressão 3D, Biotintas, Hidrogéis, Pectina, Nanofibras de Celulose, Engenharia de tecidos

resumo

A implementação de estratégias personalizadas e eficientes para a regeneração de tecidos/órgãos danificados é cada vez mais importante, e nos últimos anos têm-se observado avanços significativos no campo da engenharia de tecidos, nomeadamente, na bio-impressão 3D de análogos de tecidos vivos funcionais. Esta tecnologia automatizada permite o controlo do ambiente celular e também da organização tecidular. Para que o tecido impresso seja funcional e adequado para a aplicação em causa, o método de bio-impressão e a biotinta necessitam de ter propriedades e funcionalidades adequadas, sendo a sua seleção um passo fundamental. Recentemente, tem havido um grande progresso no desenvolvimento de biotintas para aplicação em bio-impressão 3D. Contudo, as biotintas desenvolvidas ainda apresentam diversas limitações, tais como fracas propriedades mecânicas, baixa viabilidade celular ou custos de produção elevados.

Neste contexto, o objetivo desta dissertação é o desenvolvimento de uma biotinta à base de um hidrogel de pectina e nanofibras de celulose (NFC) com incorporação de queratinócitos humanos (células HaCaT) para aplicação em bio-impressão 3D. Estes biopolímeros foram escolhidos devido às suas propriedades intrínsecas e ao seu potencial para impressão 3D. A pectina é biodegradável, hidrofílica e forma hidrogéis na presença de catiões divalentes, como o cálcio. A nanocelulose também já demonstrou as suas potencialidades, revelando excelentes propriedades mecânicas e biocompatibilidade. Contudo, a combinação de pectina e NFC nunca fui explorada no campo da bio-impressão 3D.

As tintas desenvolvidas foram caraterizadas em termos da sua reologia, estrutura/composição química e morfologia. Adicionalmente, os parâmetros de impressão foram otimizados e a citotoxicidade dos hidrogéis avaliada. Reologicamente, as tintas apresentaram um comportamento pseudoplástico, que é extremamente importante para aplicações em bio-impressão 3D e, além disso, após pré-reticulação observou-se um aumento de três níveis de magnitude na viscosidade e tensão de cisalhamento. As tintas desenvolvidas têm aptidão para serem imprimidas, tendo o resultado mais promissor sido obtido para a tinta com maior quantidade de NFC e pré-reticulada com 1% (m/v) de $CaCl_2$. Nomeadamente, conseguiu-se imprimir até 8 camadas sem perder resolução. Os hidrogéis imprimidos mostraram ser não citotóxicos para as células HaCaT, contudo os valores de viabilidade celular mais elevados foram observados para os hidrogéis com maiores quantidades de nanocelulose. Este estudo considera-se como um grande passo em direção ao uso de biotintas baseadas em pectina e NFC em bio-impressão 3D.

keywords 3D-Bioprinting, Hydrogels, Pectin, Cellulose Nanofibers, Tissue Engineering,

abstract

The implementation of personalized and efficient strategies for damaged tissue/organ replacement is becoming increasingly urgent, being observed significant advancements in the field of tissue engineering in recent years, namely in 3D bioprinting of functional living tissue analogues. This automatized technology allows a wide control over the cellular environment and the overall tissue organization. To obtain a fully developed and functional tissue/organ, the bioprinting method and the bioink need to have adequate properties and functionalities, for this reason, a thoughtful choice is crucial. Recently, there have been great developments in the field of bioinks for bioprinting applications. However, the developed bioinks still present several limitations, such as weak mechanical properties, low viability, or high production costs.

In this context, the objective of this dissertation is the development of a pectin-nanocellulose fibers hydrogel-based bioink laden with human keratinocyte cells (HaCaT cells) for 3D bioprinting. These biopolymers were chosen due to their great potential for 3D bioprinting applications. Pectin is biodegradable, hydrophilic, and can form hydrogels in the presence of divalent cations, such as calcium. Nanocellulose has also already demonstrated its potentialities in 3D-bioprinting, revealing excellent mechanical properties and biocompatibility. However, this combination of biopolymers has never been explored for 3D-bioprinting. The developed bioinks were characterized in terms of their rheology, chemical structure/composition, and morphology. Furthermore, the bioprinting parameters were optimized and the cytotoxicity of the hydrogels evaluated. Rheologically, the inks presented a shear-thinning behavior, which is extremely important for 3D bioprinting applications, furthermore, an increase of three levels of magnitude in viscosity and shear stress was observed after a pre-crosslinking procedure. The inks were able to be printed with the optimal result being obtained for the ink with the highest content of NFC and pre-reticulated with 1% (m/v) $CaCl_2$, which allowed the printing of up to 8 layers without losing resolution. The fully-crosslinked hydrogels were considered non-cytotoxic towards HaCaT cells, however higher cell viability values were observed for the hydrogels with higher NFC content. This study can be considered a great step towards the use of pectin-NFC-based bioinks in 3D-bioprinting applications.

Table of Contents

Abbreviations

µ-CT – Micro-computerized tomography

2PP – Two-photon polymerization

BCE – Before Common Era

CAD – Computer-aided design

DBB – Droplet-based bioprinting

dECM – Decellularized extracellular matrix

DMEM – Dulbecco's modified eagle medium

DMSO – Dimethyl sulfoxide

EBB – Extrusion-based bioprinting

ECM – Extracellular matrix

EHD – Electrohydrodynamic bioprinting

FTIR –ATR – Fourier transform infrared-attenuated total reflection spectroscopy

GAGs – Glycosaminoglycans

GelMA – Gelatin methacrylate

LBB – Laser-based bioprinting

LDW – Laser-based direct writing

MRI – Magnetic resonance imaging

MSC – Mesenchymal stem cell

MTT – 3-(4,5-Dimethylthiazol-2-yl)-2,5-diphenyl tetrazolium bromide

NFC – Cellulose nanofibers

PCL – Polycaprolactone

PEG – Polyethylene glycol

PEO – Polyethylene oxide

PPO – Polypropylene oxide

ROP – Ring-opening polymerization

SDS – Sodium dodecyl sulfate

SEM – Scanning electron microscope

SLA – Stereolithography

UNOS – United Network for Organ Sharing

UV – Ultra-violet

List of Figures

List of Tables

1.Introduction

The data provided by the United Network for Organ Sharing (UNOS) clearly shows that the demand for organ transplants in the United States of America is much greater than the supply. As of September 2019, in the UNOS records, there were a total of 112.861 humans needing a transplant for which there were only 12.742 donors signed. Although the number of transplants and donors is at its peak, with over 26 thousand transplants performed from January 2019 to August of the same year, there is a need for customizable and on-demand strategies.[1]

Tissue engineering uses living cells, biocompatible materials, and biochemical/physical factors to create tissue-like constructs, targeting primarily the reparation of injuries and ultimately, the replacement of a failing organ's function.[2] Additionally, tissue-like constructs can also be used for studies of tissue development and morphogenesis and even drug testing efficacy and toxicology. Historically speaking, the first time that this technique has been used dated back to 3000 BCE (Before Common Era) when Indians described skin grafting practices.[3] However, the first successful tissue-engineered skin products were produced in the late 1970s and early 1980s. One of the most important studies to date was published in 1997 where it was shown that it was possible to rebuild the cartilaginous tissue of a 3-year old child's ear on a mouse (Figure 1).[4] This approach introduced tissue engineering to the world, resulting in a higher interest from the scientific community. Over time, a need to fabricate custom-made scaffolds started to rise. This led to the development of microscale technologies, such as 3D bioprinting, that offer a wide control over the cellular microenvironment and the overall tissue organization and spatial structure, with the addition of being automated.[5]

Figure 1 - Representation of the subcutaneous implantation of chondrocytes on a poly(lactic-co-glycolic acid) template and their further development into a human's ear shape in a nude mouse. Adapted from Cao Y, *et al*. (1997).[4]

To engineer living tissues using 3D bioprinting, there is a need to develop and utilize bioactive living tissue constructs capable of providing essential growing conditions to the cells previously enclosed into them.[6] These constructs are designed and developed by means of computer-aided design (CAD) using, as reference, data from medical imaging techniques, such as X-Ray, magnetic resonance imaging (MRI), and micro-computerized tomography scan (μ-CT- scan). They are developed in a way that allows the cells to grow and differentiate into, firstly, a tissue and desirably a working organ. The development of these constructs is made possible through the deposition, layer by layer, of cell-laden biomaterials by a 3D bioprinter.[6] This approach grants us the ability to personalize patent-specific designs, as well as on-demand creation of high precision and complex structures within a short period. The cell-laden biomaterials that are printed are named bioinks and can be split into two major types, scaffold-based and scaffold-free bioinks. The bioinks need to be easily produced and processed whilst maintaining an affordable price and being commercially available. Even though there is a need to minimize the production cost and industrial complexity, these materials need to maintain certain mechanical and biochemical properties that are essential to cell survivability and the technique's overall success. During the development of bioinks, several characteristics are strived for, namely the ability to maintain the shape and structural integrity after printing, ease of engraftment with the host and grade of degradation over time, non-immunogenicity, and non-toxicity.[7]

1.1. Bioprinting methods

The 3D bioprinting approach can be described, as previously referred, as a computer-aided (CAD) process to arrange and assemble living and non-living materials in a previously defined 2D or 3D organization, so that they can form bioengineered structures that can be applied in the fields of regenerative medicine, pharmacokinetic and cell biology.[8] There are several bioprinting methods with their own applications and limitations. It relies on the user to define which approaches are the most favorable depending on the intended purpose. The bioprinting methods featured in this review are, extrusion-based (EBB), droplet-based (DBB), laser-based (LBB), and stereolithography (SLA).[9] Other bioprinting systems are microvalve-based bioprinting[10], two-photon polymerization (2PP)[11], and microfluidic printing[12].

Depending on the bioprinting method, the forces applied when printing can lead to cell necrosis, resulting in decrement of tissue density. Different bioprinting methods have different cell viability outputs, DBB, LBB, and SLA techniques have more than 85% of cell viability whereas EBB results in 40%-80% cell viability.[13]Additionally, not every technique can print bioinks with high cell density. For instance, DBB can deliver low cell densities bioinks (< 10^6 cells/mL), LBB and SLA can go up to medium cell densities (< 10^8 cells/mL) and EBB allows bioprinting of the highest cell density bioinks and even cell spheroids.[13] In sum, cell density and viability are crucial factors in choosing the bioprinting method for each bioink and application.[14]

1.1.1. Extrusion-based bioprinting (EBB)

The extrusion method relies on dispensing a bioink, previously loaded in a tube, through a micro nozzle following pre-determined commands from a computer design program. This technique achieves a much higher precision (200 μm) than droplet-based or even laser-based techniques.[15] The downside is the slower fabrication speed when compared to the other two main techniques.[16] The movement and allocation of the bioink are made possible through a compressor that exerts force using pneumatic, piston, or screw mechanisms (Figure 2). Every single mechanism has its own advantages and disadvantages. The pneumatic system is characterized by a delay in the deposition due to the compressed gas, however, it finds its best use with highly viscous molten polymers systems. The piston-driven system has the best performance regarding the control of the deposition.[17] Ultimately, the screw-driven system has a higher spatial control and is commonly used in the deposition of high viscosity hydrogels. This method, when using common screws, generates a larger pressure on the nozzle which can be injurious for the bioink's cell viability. This issue can be addressed by designing/picking up a specific screw for the application in mind.[15]

A multi-head tissue/organ building system (MtoBS), was developed to dispense a wide range of biomaterials. However, a major disadvantage of this system is the need to print one material at a time, slowing down the process. Afterwards, it was developed a bioprinter with two independent arms that can lay down multiple bioinks at the same time, speeding up the process.[9]

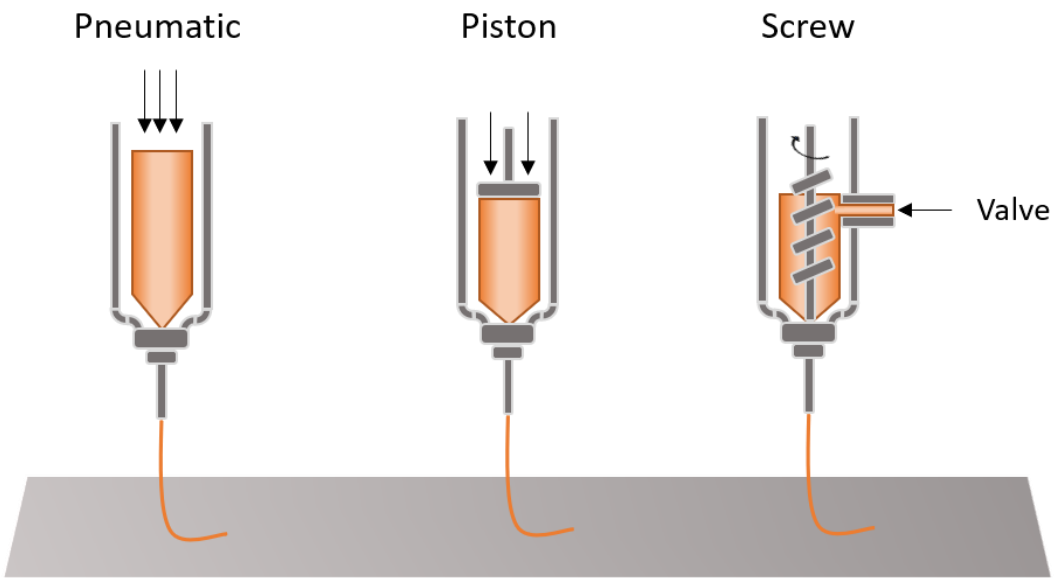

Figure 2 - Representation of extrusion-based bioprinting modalities.

1.1.2. Droplet-based bioprinting (DBB)

Droplet-based bioprinting is a simple, versatile, agile, and highly controllable technique based on the manipulation of the bioink in such a way that it forms droplets. These droplets are obtained by exposing the bioink to a couple of conditions, such as the force exerted by gravity and atmospheric pressure. Manipulating the fluid mechanics namely viscosity and surface tension allows for the creation of more precise and higher resolution bioconstructs.[18]

This technique offers several advantages over the other bioprinting techniques. The first is the ability to produce highly complex tissue constructs with different cells in their composition. In fact, EBB is characterized by a higher difficulty to generate heterocellular constructs and, in LBB, it is challenging to incorporate multiple types of bioactive molecules. Additionally, DBB offers a better printing resolution, by mediating the gelatinization process, and enables control over certain properties, such as swelling and shrinkage of the construct, resulting in a more predictable geometry and size of the final product.[18] It also allows for rapid fabrication of arrays of samples, which is highly desirable in applications as, drug and cancer screening.

However, DBB has a major limitation, known as clogging. Due to the high viscosity of some bioinks, the bioink accumulates and leads to obstruction of the nozzle, which typically has a diameter of 10 to 15 μm. The workaround requires the use of

bioinks based on hydrogels, due to their low viscosity.[18] Some other limitations that are worth noting are the inability to create mechanically strong and structured constructs due to the limited availability of compatible bioinks and also the difficulty to fabricate porous tissue constructs.[9]

This bioprinting technique can be split into three major categories namely, inkjet, acoustic and electrohydrodynamic printing (Figure 3).[18] Inkjet printing is based on a simple process that uses the force of gravity or atmospheric pressure combined with fluid mechanics to form the droplets. As it stands it can also be divided into three categories depending on the method used, namely electrostatic inkjet bioprinting, thermal inkjet bioprinting, and piezoelectric inkjet bioprinting.[18] Electrostatic inkjet bioprinting generates droplets due to a voltage pulse that bends a pressure plate increasing the volume of the ink chamber, resulting in the ejection of a single droplet. In thermal inkjet printing, a thermal actuator heats the ink, forming an air bubble. This bubble expands and explodes rapidly, generating a quick variation of the chamber's pressure leading to the ejection of a droplet. Lastly, piezoelectric inkjet printing relies on the form-changing factor of the actuator that happens when it is struck by a voltage pulse. This change in shape will cause a deformation of the fluid chamber and, consequently, it will affect its volume. This will lead to the formation of a pressure wave that causes the droplet to be released.[18]

Acoustic bioprinting has the advantage of not exposing the ink's cells to harmful stressors like the ones presented in inkjet bioprinting, namely voltage, pressure, and heat. This technique is often composed of an open pool of bioink held in place due to the surface tension at the exit channel. To eject droplets an acoustic actuator composed of a piezoelectric substrate and interdigitated gold rings generate acoustic waves ,which will form an acoustic focal point near the exit channel, disturbing the surface tension and leading to the ejection of such droplets.[18,19]

Electrohydrodynamic (EHD) bioprinting has the advantage of not exposing the ink to harmful conditions. This is accomplished by using an electric pulse, originated from the high voltage applied between the nozzle and the substrate, to generate electrostatic stresses stronger than the surface tension of the nozzle's orifice in order to pull the bioink through the nozzle, neglecting the need for high pressure. Due to this, EHD is ideal for applications that require small nozzles and high viscosity/concentration bioinks. Another advantage of this method is that it enables the user, depending on the

voltage, to choose a specific droplet stream mode. Cell viability post-printing is not only affected by the electric field but also by the bioink flow rate and the ink's properties, such as cell type and concentration.[20]

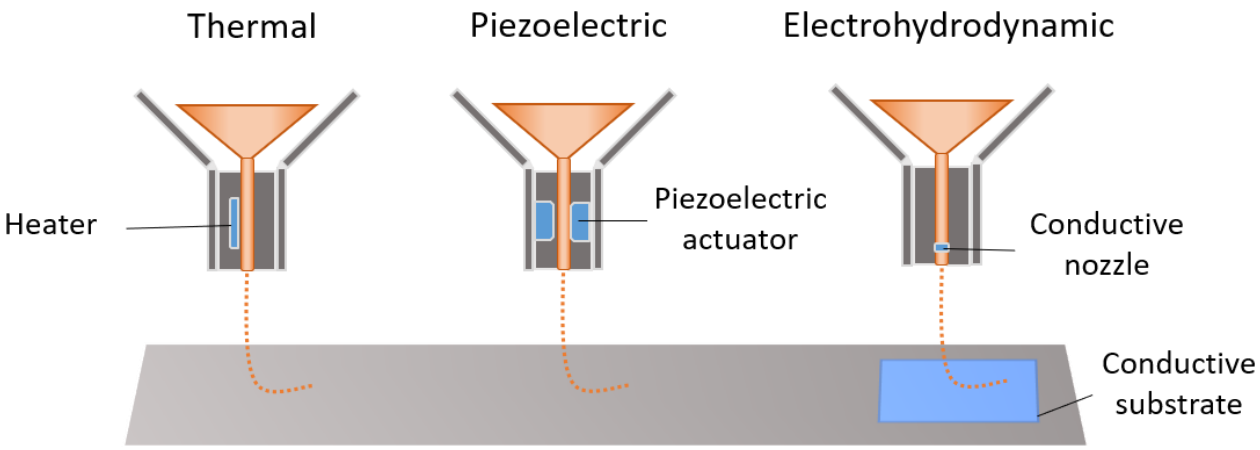

Figure 3 - Representation of droplet-based bioprinting modalities.

1.1.3. Laser-based Bioprinting (LBB)

Laser-based bioprinting is founded on the use of a laser pulse to transfer cell-laden droplets from the donor slide to a collector slide (Figure 4). This transfer occurs after the creation of a bubble due to a laser pulse. Consequently, the formation of these bubbles will generate shockwaves that will propel the cell from the donor to the collector slide. The most common biofabrication method based on laser is named Laser-based direct writing (LDW), a method that can rapidly create precise patterns while maintaining cell viability. As in every bioprinting method, it also has its advantages and disadvantages. The major advantage of this bioprinting method is focused on its nozzle-free nature, allowing the use of high viscosity bioinks (in opposition to Inkjet and EBB). It also offers high-precision printing, which is essential for the development of an organ's smallest characteristics. Regardless of the advantages of laser bioprinting, the heat generated from this procedure may affect cell viability and intercell communication/aggregation. It also faces the downfall of having a prolonged fabrication time and demands photocrosslinkable materials (materials able to form photoinduced covalent bonds with each other).[21]

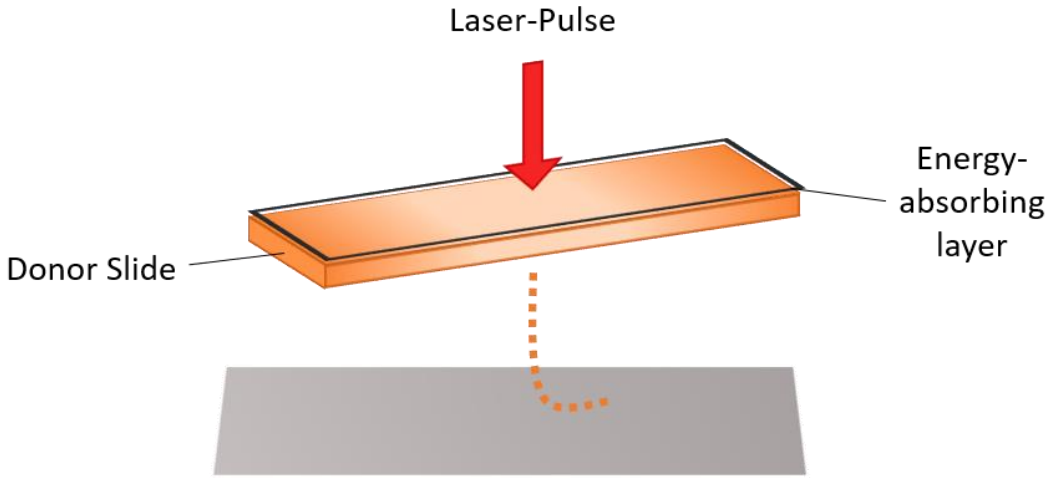

Figure 4 - Representation of laser-based bioprinting modality.

1.1.4. Stereolithography Bioprinting (SLA)

Stereolithography is a light-assisted printing method that uses ultra-violet (UV) light in order to photo-polymerize liquid resins, generating thin layers of solid material. After the polymerization of a layer, the structure moves, either *Bottom-up* or *Top-down*, allowing the formation of another layer.[8] Consequently, the latter layer is going to adhere to the previous one, resulting in a 3D physical structure (Figure 5). Whenever the UV light strikes the light-sensitive bioink (resin) it promotes the formation of crosslinks between the bioink's macromolecules generating a stable 3D structure. This method allows a high-fidelity control on the porosity, resolution, and mechanical properties of the finished products. However, this technology has several limitations, viz. the use of UV light has a detrimental effect on the cell's nuclear DNA and overall cell viability;[8] unsuitable for high mechanical load applications since it produces rigid and fragile constructs; high material cost added up with expensive and complex equipment. Moreover, since it is in the development stage, there are still few light-sensitive bioinks to choose from.[14,22]

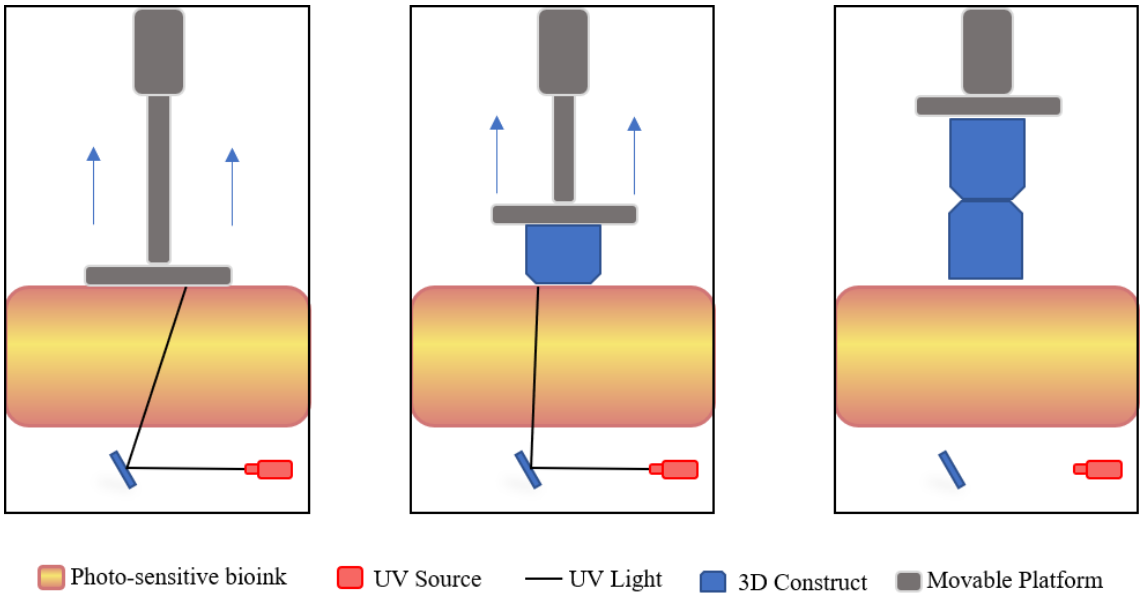

Figure 5 - Representation of stereolithography modality; (Sequential order from left to right).

1.2. Types of Bioinks:

Alongside the selection of the bioprinting method, bioinks are also an essential component in the functionality and success of the 3D bioprinting procedure. Their selection depends on the predetermined application, the type of cells, and the bioprinter used.[23]

Following the importance addressed in the latter statement and as previously referred, bioinks can be divided into two major types: scaffold-based and scaffold-free bioinks. The first type consists of the loading of cells into an exogenous material, including hydrogels, microcarriers, and decellularized matrix components. And, the latter involves 3D bioprinting of the cells without the use of any supportive exogenous material, in a way that resembles embryonic development.[6] To be considered functional, a bioink needs to be biocompatible, i.e. it needs to have the ability to persist in the organism without causing damage to the cells that can result in scarring or cause a response that detracts from its desired function.[24] Next, it will be briefly presented and discussed each bioink type, their characteristics, and advantages/disadvantages.

1.2.1. Scaffold-free bioinks

Scaffold-free bioinks mimic embryonic development through cellular self-assembly mechanisms. Organizing the cells in a three-dimensional structure allows

them to develop and differentiate into a tissue when compared to a regular cell monolayer. To obtain these three-dimensional structures, certain cell types, such as epithelial cells, can form aggregates by bounding themselves with cadherin molecules and by secreting their own extracellular matrix (ECM).[25,26] These cadherin molecules will promote strong intercellular adhesion and enable signal transduction, increasing integrin expression. Finally, integrins will allow the cell's cytoskeleton to adhere to the ECM, leading to a fully developed cell structure and, later, a tissue.[7] This can also be observed with the cells that will be subject of the present study, keratinocytes.[27] There are three main types of scaffold-free bioinks namely tissue spheroids, cell pellets, and tissue strands.

1.2.1.1. Tissue spheroids

Tissue spheroids represent spherical scaffold-free aggregates of cells with a diameter of 200 to 400 μm. Out of the three main scaffold-free techniques, this is the most gentle and thus induces much less or no cell damage.[25] These bioinks can only be printed using extrusion-based bioprinters (EBB).

There are quite a few alternative techniques to produce tissue spheroids, one of the most popular is culturing cells in microwells previously cast on non-adhesive hydrogels. In this technique, a computer program designs micro-molds that will be later cast on the hydrogel creating arrays of microwells, whenever the cells are seeded on these microwells, they will drop to the bottom and contact with each other stimulating the cadherin production and cell's aggregation, resulting in the consolidation of the tissue.[7] Another well-known technique is the hanging-drop technique where a small volume (15 – 30 μL) of cells is placed on a petri dish that, afterwards, gets inverted. Due to gravity and surface tension, the cells start to form two-dimensional aggregates (cell spheroids) at the lower border of the droplet that can be harvested using a pipette.[8,28] Figure 6 shows some examples of tissue spheroids and how they behave during and post-printing.

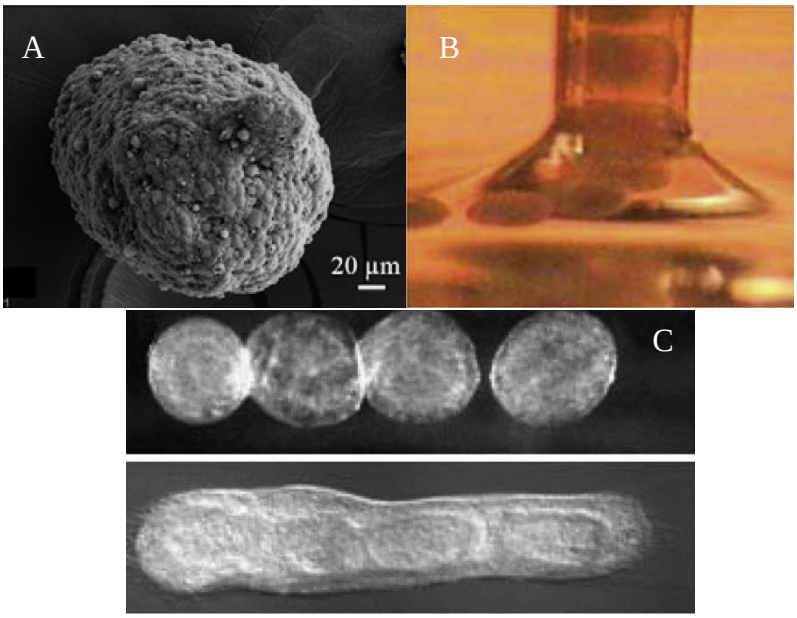

Figure 6 – Bioprinting of tissue spheroids. (A) Tissue spheroids made of rat endothelial cells (Adapted from Hospodiuk *et al*., 2017).[7] (B) Tissue spheroids during printing; (C) Fusion of several tissue spheroids after printing (Adapted from Mironov *et al*., 2009).[29]

1.2.1.2. Cell pellet

The cell pellet is a bioink type that is obtained through the exposure of cells to a gravitational or centrifugal force, leading to their deposition at the bottom of a conical tube. Subsequently, these cells can be extracted and transferred to a molding structure, where they will be able to establish intercellular interactions resulting in a more cohesive structure.[7] This technique offers a way to generate cell aggregates without using advanced systems, however, it generates agglomerates with limited oxygen and medium circulation resulting in a less viable cell culture after twenty-four hours. Similarly, to tissue spheroids bioinks, this one is also used only with EBB.[7] Figure 7 shows the stages of bioprinting a cell pellet, from the loading of the nozzle to the final printed product.

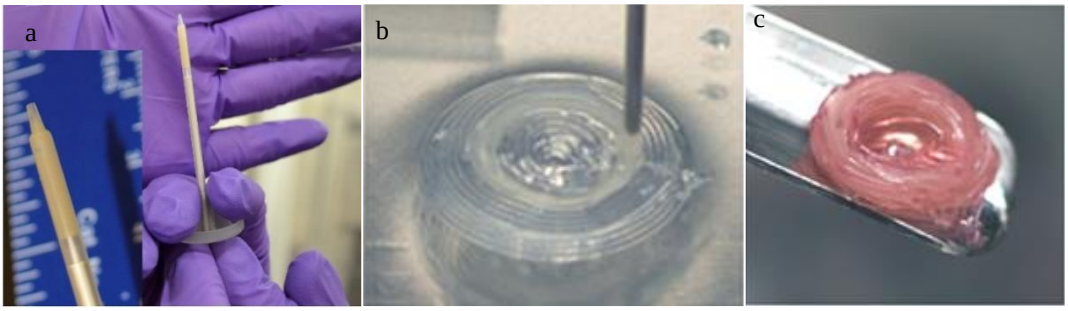

Figure 7 – (a) Cell pellet located at the tip of the nozzle (Adapted from Dababneh, A. *et al*., (2014))[9]; (b) Cell pellet being printed in an agarose mold to mimic aortic vessels. (c) A 3D bioprinted aortic construct made of cell pellet that resulted from the printing process seen in (b) (Adapted from Kucukgul *et al*., 2014).[30]

1.2.1.3. Tissue strands

The last type of scaffold-free bioink is obtained through the formation of tissue strands. These strands are obtained through micro-injection of a, previously extracted, cell pellet into a micro-tubular system, consisted of tubular permeable alginate capsules.[31] Here, the cells will develop and multiply, inheriting the tubular shape and resulting in a cylindrically shaped tissue. These fused bodies of cells will then be engineered and loaded into a bioprinter head based on a coaxial nozzle system. This procedure offers a safe and favorable environment for the cells as it maintains considerable cell viability (up to 90%).[32] Moreover, it also ensures rapid tissue strand fusion resulting in a faster formation of an entire unit. It has been reported that this procedure produces tissues with a high degree of ECM deposition when developing cartilage tissues, meaning that it can produce viable tissues.[31] Despite being such a favorable technique, the need to use such a high quantity of cells drives the procedure to be more laborious and all-around more costly. Figure 8 highlights the development of tissue strands in a tubular system, its printing process and post-printing tissue behavior.

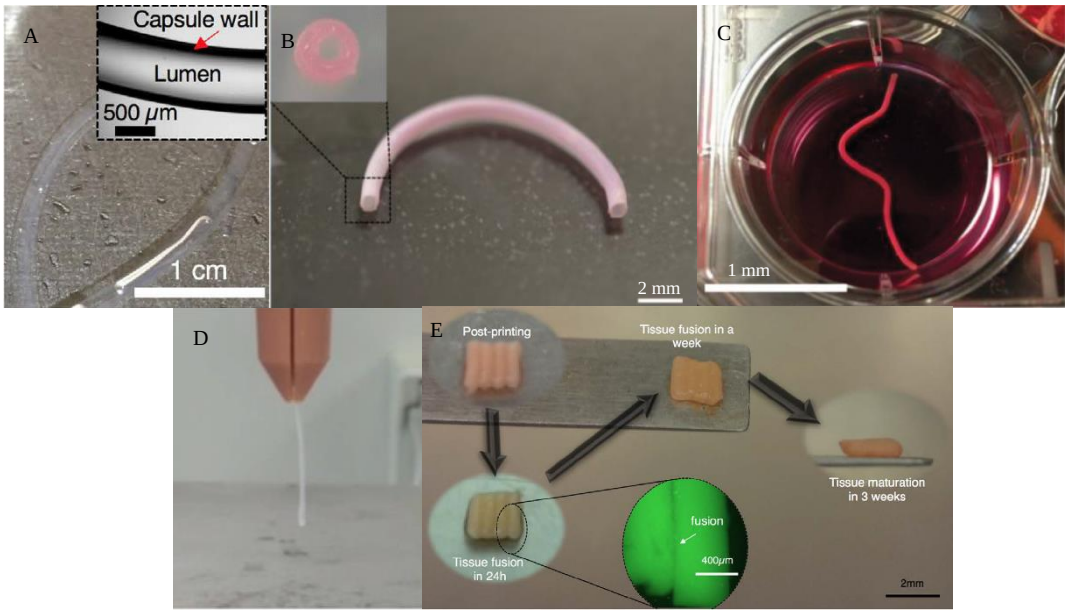

Figure 8 – Tissue strand fabrication and development. (A) An alginate tubular conduit developed to shape the cell pellet into tissue strands; (B) A cultured tubular conduit; (C) Tissue strand made of mouse insulinoma cell pellet after releasing from the tubular conduit; (D) Printing process; (E) Printed tissue development over 3 weeks; (Adapted from Yu *et al*., 2016).[31]

1.2.2. Scaffold-based bioinks

In a scaffold-based approach, the printing of the 3D structure is carried out using a bioink composed of living cells and a supportive biomaterial. The biomaterial encapsulates the cells and over time it will degrade allowing the cells to expand and form a structured tissue. There are three main types of scaffold-based bioinks namely decellularized matrix components, microcarriers, and hydrogels.

1.2.2.1. Decellularized matrix components

Cells produce and secrete specific molecules that will eventually lead to the development and formation of ECM, an intercellular medium that provides support, regulates intercellular communication, and allows the cells to adhere to each other.[7] To obtain a decellularized extracellular matrix (dECM), which can be used to develop bioinks, typically requires a purification protocol on the ECM. This protocol dwells into the removal of cellular material by using chemical/enzymatic, physical, or combinative processes.[7] For instance, to decellularize a cadaveric heart of a rat, the use of sodium

dodecyl sulfate (SDS) and polyethylene glycol (PEG) resulted in more efficient decellularization than that obtained with enzymatic processes.[33] Despite being the most widely used, chemical and enzymatic processes can induce cytotoxicity which can lead to matrix protein destruction. Due to this, mechanical processes have been developed and start to rise as an alternative.[34] Lastly, the combined methods try to gather the advantages of the chemical processes with those of mechanical ones, in order to yield a dECM suitable for the desired application. The success of a decellularization depends on the removal of a certain percentage of cells, specifically about 98%.[35] Additionally, to further determine the success rate it is also necessary to measure other factors, such as elimination of genetic material that is essential to prevent immunorejection by the host's cells; preservation of proteic components with emphasis on structural proteins (collagen, fibronectin, laminin), glycosaminoglycans (GAGs) and growth factors; and retention of the original ECM mechanical properties (measured via tensile strength and elastic modulus).[34]

Bioinks based on dECM have been rising as a strong contender in the bioprinting field. Printing of this bioink type is mostly executed using custom-built extrusion-based[36] or dispensing-based[35,37] printers, however, LBB and DBB can also be used.[13,38] It has been demonstrated that dECM provides not only better cellular proliferation and tissue-function than other printable materials, but also it does not induce cytotoxicity or inflammation after *in-vivo* implantation.[7,15] Adding to the list of advantages of this bioink, it also contributes to the development of more advanced and specific tissues in place of inferior and less functional scar tissue.[39]In figure 9, a couple of dECM bioprinting products are presented.

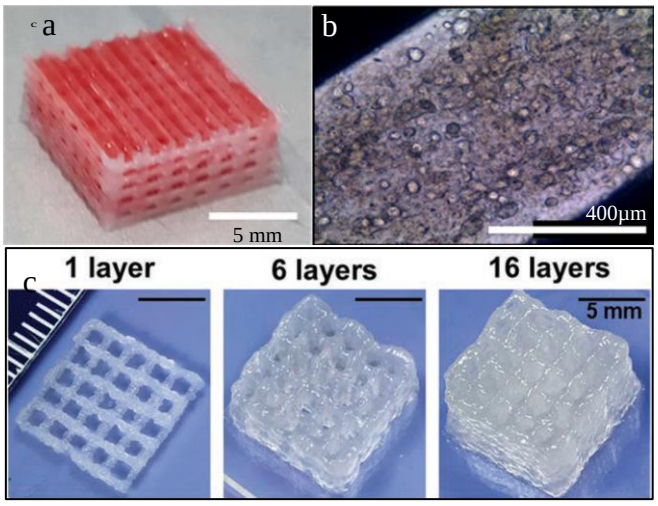

Figure 9 - Bioprinting of various dECM structures. (a) Adipose dECM and polycaprolactone (PCL) structure; (b) Microscopic image of the same cell-laden dECM structure complemented with a PCL framework. (Adapted from Pati, F. *et al*., (2014))[35]; (c) Printing outcome of a photo-crosslinkable dECM-derived construct with multiple layers. (Adapted from Ali, M. *et al*., (2019)).[40]

1.2.2.2. Microcarriers

Microcarriers are supportive structures that allow cell growth and expansion due to their spherical shape and interconnected porosities (Figure 15).[41] By having a spherical architecture these structures offer an extensive available area for cell attachment and development and a more efficient nutrient and gas transfer when compared to a 2D system.[7,42] This technology has already been widely used in pharmacological applications, such as vaccine development and cell therapy bioprocessing. They can be classified based on the material composition and the state of matter of the substance that the cells develop in. Regarding the materials, the most widely used are ceramic and polymer-based microcarriers, due to their biocompatibility, reproducibility, and mechanical properties.[43] Polymers may be natural or synthetic-based, however, synthetic polymers suffer from poorer cell adhesion than natural counterparts. Additionally, the surface properties of the microcarriers can be customized to a certain application, an example is the ability to add specific cell adhesion ligands to a microcarrier surface resulting in a different cell-host interaction.[43]

Regarding the state of matter, the microcarriers can be split into two different categories: solid or liquid state.[43] Solid microcarriers provide internal spaces for cell

attachment which is an important factor in the protection of cells against external stresses. However, solid microcarriers face three major challenges, the lack of system oxygen/nutrient transportation and the accumulation of toxic metabolites inside the structure. A liquid state interface microcarrier is based on the growth and development of cells in a liquid/liquid interface consisted of a growth medium and a hydrophobic liquid.[43] The development of more advanced liquid interfaces can be the catalyzer of the next generation of microcarriers with fewer disadvantages and it is a step forward on the production of a fully customizable and "ideal" microcarrier for different applications.

In the field of bioinks, microcarriers are mostly used as supporting structures. When embedded in hydrogel matrices, microcarriers offer mechanical reinforcement to the gel, as well as, a more expansive cell-anchoring and spreading surface.[44] Additionally, in order to further tailor the cells to application-specific needs, microcarriers can be loaded with bioactive compounds that control their spatial and temporal distributions, guiding the development and differentiation of the cells to a precise goal.[44] Due to all of this, microcarriers appear to be a great addition to help improve the viability and success of the bioprinting method. In figure 10, the printing process of a microcarrier-based bioink is shown, as well as, a immunofluorescence image of the printed structure.

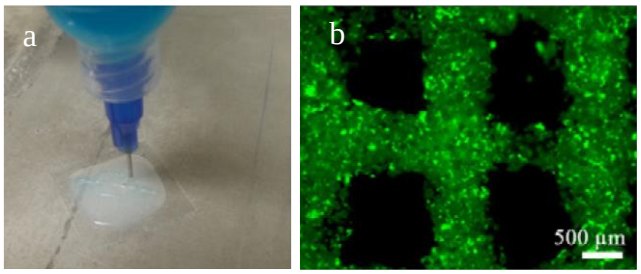

Figure 10 – Microcarriers for bioprinting. (a) Representative bioprinting of microcarrier-laden hydrogels through an extrusion-based process.; (b) Immunofluorescence staining for actin cytoskeleton of bioprinted microcarriers loaded in a gelatin methacrylate (GelMA) hydrogel matrix. (Adapted from Levato *et al*. (2014) [44]).

1.2.2.3. Hydrogels

Hydrogels are polymeric materials with the ability to absorb and retain large quantities of water without solubilizing or degrading their 3D structure.[15] The hydrophilicity is one of the main factors that determine the biocompatibility and printability of a scaffold.[6] Hydrogels are often used in the production of cell-laden structures, due to their ability to mimic the native 3D tissue environment, allowing them to encapsulate cells in a hydrated and mechanically functioning environment, leading to a higher biocompatibility rate.[45]

The 3D structures of hydrogels are maintained under different conditions, due to the physical and chemical links established between the polymeric chains. This process is denominated crosslinking and is important in the success rate of the procedure as it strongly impacts structure robusticity and longevity.[23,46] There are two types of crosslinking, physical and chemical.[7] Physically crosslinked hydrogels are typically non-cytotoxic because non-exogenous crosslinking agents are required, and as this type of crosslink is usually based on weak forces, it is considered reversible.[7,47] Physical crosslinking occurs through ionic interactions, hydrogen bonding, temperature, or pH variations.[47] An example of an ionic crosslinking mechanism is the alginate's "egg-box" model (Figure 11). This model is based on the specific interactions established between calcium ions (Ca^{2+}) and the guluronate molecules of the alginate molecular backbone.[48] These interactions will group the guluronate chains resulting in a compact structure, an alginate hydrogel.[8]

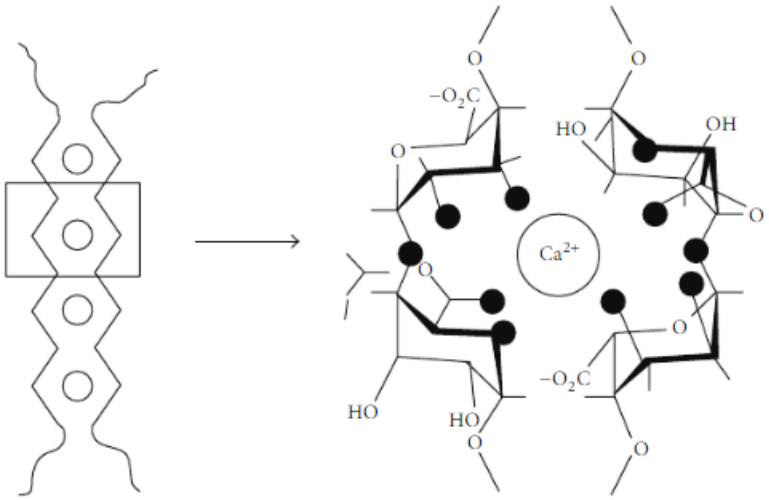

Figure 11 - "Egg box model". Schematic drawing with a further in-depth view of the structure formed by the strong electrostatic interaction between the calcium cation and the guluronate strands. The dark circles represent the oxygen atoms involved in the interaction with the calcium ion. (Reproduced from Braccini, I. *et al*., (2001)).[49]

On the other hand, chemical crosslinking presents more stability, durability, and better mechanical properties when opposed to physical crosslinking. This crosslinking mechanism is based on the formation of covalent bonds between different polymer chains, this is achieved by using a crosslinking agent with specific functional groups, such as aldehydes, or by the formation of reactive species due to high energy irradiation viz, ultra-violet, microwave, or gamma.[7,15,47] Consequently, the use of an exogenous crosslinking agent or the generation of reactive species, can lead to cytotoxicity and endanger cells.[50]

Hydrogels are commonly divided into two main categories, natural or synthetic based, according to the nature of the polymers used to produce them (Figure 12).[51] Natural hydrogels can be further classified as protein-based, polysaccharide-based, and decellularized hydrogels.[51]

Over the years, hydrogels have been gaining popularity in the 3D bioprinting field. In table 1 it is summarized some of the most common hydrogel-based bioinks and their applications.

Table 1 – Examples of hydrogel-based bioinks used to date. Adapted from (Gungor Ozkerim et al. 2018).[23]

Biomaterial	Origin	Bioprinting method	Cells used	References
Poloxamers	Synthetic	Extrusion-based	Bovine chondrocytes	[52]
PEG**	Synthetic	Extrusion-based	Human Mesenchymal Stem cells (hMSCs)	[46]
		Extrusion-based	Mouse embryonic fibroblast cells (3T3)	[53]
		Inkjet modified	hMSCs	[54]
PCL***	Synthetic	Extrusion-based	hMSCs	[55]
		Extrusion-based	Mouse osteoblastic cells (MC3T3-E1),	[56]
		Inkjet-based	Rabbit Chondrocytes	[57]
GelMA****	Semi-Synthetic*	Extrusion-based	Cardiomyocytes and fibroblasts	[58]
Chitosan	Semi-Synthetic*	Inkjet-based	Macrophages	[59]
Gelatin	Natural	Extrusion-based	Cardiomyocytes, fibroblasts,	[60]
		Extrusion-based	Human liver cancer cell line (HEP-G2),	[61]
		Extrusion-based	hMSCs and Chondrocytes	[62]
Collagen	Natural	Laser-based	Fibroblasts, Keratinocytes,	[63]
		Laser-based	Fibroblasts, Keratinocytes	[64]
		Droplet-based	Smooth Muscle Cells,	[65]
		Extrusion-based	Preosteoblasts and Human adipose Stem cells (ASCs).	[66]
Alginate	Natural	Extrusion-based	Cartilage progenitor cells,	[67]
		Extrusion-based	Mouse fibroblasts,	[68]
		Laser-based	3T3	[69]
		Inkjet-based	3T3	[70]
Fibrin	Natural	Inkjet-based	ASCs and endothelial colony-forming cells	[71]

*Semi-Synthetic, obtained by modification of a natural polymer. ****PEG** – Polyethylene glycol
*****PCL** – Polycaprolactone ******GelMA** – Gelatin methacrylate

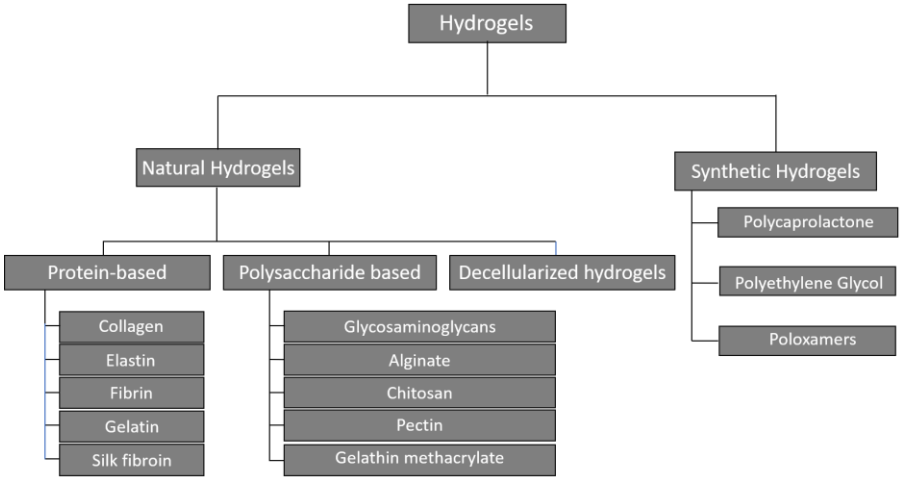

Figure 12 – Schematic representation of the classification of most used types of hydrogels.

Synthetic hydrogels (Table 1 and Figure 12) are usually produced using, poloxamers (Pluronic®),[52] a class of synthetic block copolymers which consist of polyethylene oxide (PEO) and polypropylene oxide (PPO) blocks;[72] polyethylene glycol (PEG),[46,53,54] a synthetic polyether that can be prepared in a wide range of shapes and conjugated with a large array of biomolecules such as, enzymes, proteins, and liposomes;[7,8] polycaprolactone (PCL),[55–57] an aliphatic polyester that can be prepared not only by condensation of 6-hydroxyhexanoic acid but also from ring-opening polymerization (ROP) of caprolactone.[7,8,55–57] However, synthetic hydrogels present several limitations such as low cell proliferation, low adhesion, and unknown long-term effects on cells.[73] To overcome such limitations, natural hydrogels, consisted of proteins, polysaccharides, or extracellular matrix (ECM) components, are emerging in this field by coming up with higher biocompatibility, biodegradability, and cellular attachment.[51,65] However, natural-based hydrogels developed so far also present several limitations, namely weak mechanical properties, high batch to batch variability, and high biodegradability.[15,51,74] On the other hand, synthetic hydrogels by having a fully tailorable production avoid these disadvantages.[15] In this sense, the combination of synthetic and natural polymers started to rise in popularity, in order to merge the advantages of synthetic and natural hydrogels.[75] Such hydrogels have been shown to preserve the intrinsic biocompatibility of the latter with the addition of the benefit of the tunability of the synthetic ones.[75] This tunability allows the modification of the hydrogels for specific applications with some of the benefits being, prevention of post-

printing distortion by adding chemical crosslinks and even, obtaining higher biocompatibility by adding biologically active compounds, such as covalently bond growth-factors or cell-adhesive compounds.[15,76] For instance, Hong *et al.*[46] developed a PEG-alginate hydrogel with a high malleability and, simultaneously, tougher than natural cartilage. PEG and alginate were chosen due to their ability to form an interpenetrating network with high mechanical strength while allowing cell encapsulation.[46] Additionally, nanoclay particles were incorporated into the PEG-alginate hydrogel to further control the viscosity of the solution before the printing process. Through an extrusion-based bioprinting process it was possible to obtain the desired 3D-printable, tough and highly adequate for long-term cell culture scaffold (Figure 13).[46]

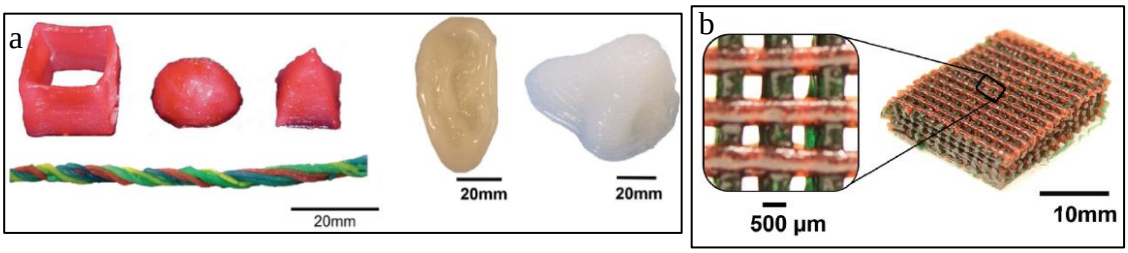

Figure 13 – Printing results of PEG-alginate-nanoclay hydrogels. Several hydrogel constructs with different shapes (a); PEG-alginate-nanoclay 3D-printed mesh (b). Adapted from Hong, S. *et al*. (2015).[46]

Chitosan,[59] gelatin,[60–62] collagen,[63–66] alginate,[67–70] and fibrin[71] are common biopolymers used to produce natural based hydrogels for 3D bioprinting (Figure 12 and Table 1). Chitosan is a biodegradable and biocompatible polysaccharide obtained from partial deacetylation of chitin, a biomacromolecule widely present in nature.[77] Additionally, chitosan can be metabolized by certain human enzymes, mainly lysozymes.[23,78] Because of these properties, chitosan is usually applied in wound dressings, drug delivery, and tissue repair. In bioprinting applications, due to its weak mechanical strength, chitosan is often coupled with other biopolymers such as alginate, agarose, and gelatin.[78] For instance, a study reported the effects of a human mesenchymal stem cell (MSC)-laden agarose-chitosan hydrogel, printed using an extrusion-based technique, and their following differentiation into osteogenic or adipogenic lineages (Figure 14).[79] However, the agarose-chitosan hydrogel didn't match

the expectations by displaying low mechanical stability due to the high porosity observed in these constructs, resulting in a loss of form after 24 h.[79]

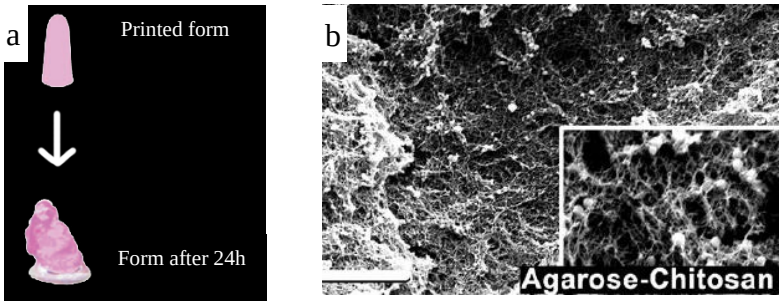

Figure 14 – (a) Agarose-chitosan hydrogel printability test where after 24 h the structure could not retain its form (b) porous microstructure of the cell-free agarose-chitosan hydrogels. Adapted from Duarte Campos *et al*. 2015.[79]

Another strategy used to improve the mechanical properties of natural based hydrogels is the reinforcement with fibers. These fibers can be natural, such as cellulose, alginate, spider silk, and collagen, with the intrinsic advantages of natural based materials; or they can be synthetic, including polymeric fibers (i.e. polyamides and polyesters), glass, and crystalline ceramic fibers, where characteristics can be tailored for a specific application.[80]

Regarding synthetic fibers, PCL is commonly used as an organized, high porosity reinforcing structure.[81] These PCL fibers have been produced through electrospinning and then combined with GelMA, a photopolymerizable derivative of gelatin, in order to print and develop a stiff hydrogel nanocomposite.[23,81] (Figure 15)

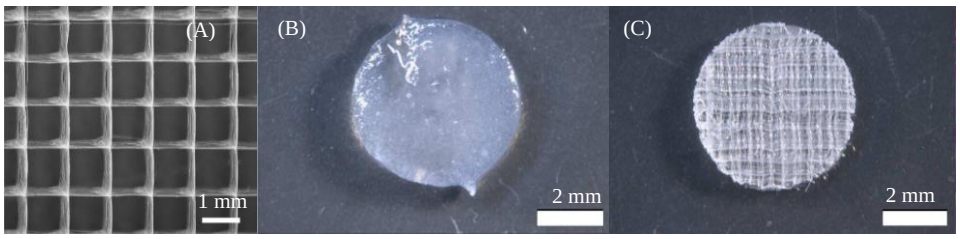

Figure 15 – (A) PCL microfibre structure; (B) Visual image of a GelMA hydrogel without PCL; (C) Visual image of a GelMA hydrogel after addition of PCL scaffold. (Adapted from Visser, J. *et al*., 2015).[81]

Cellulose, the most abundant polymer obtained from renewable sources, is mostly extracted from wood,[82] however, it can also be obtained from other life-forms,

including fungi, algae, and bacteria.[80,83] Due to its unique properties and high abundance, cellulose is used in a broad range of applications, with paper production, textiles, and more recently the production of biocomposite materials, which is the most relevant example.[82,84] Moreover, the emergence of nanometric forms of cellulose, namely nanofibrillated cellulose (NFC), cellulose nanocrystals (CNCs) and bacterial cellulose (BC), has allowed the application of cellulose in wider areas, including 3D-bioprinting.[84,85]

For example, Markstedt *et al.* (Figure 16) described the development of a bioink of alginate reinforced with nanocellulose fibrils with the objective of 3D bioprinting human chondrocytes. This procedure resulted in a biocompatible, high fidelity, and stable bioink with optimal mechanical and rheological properties.[86]

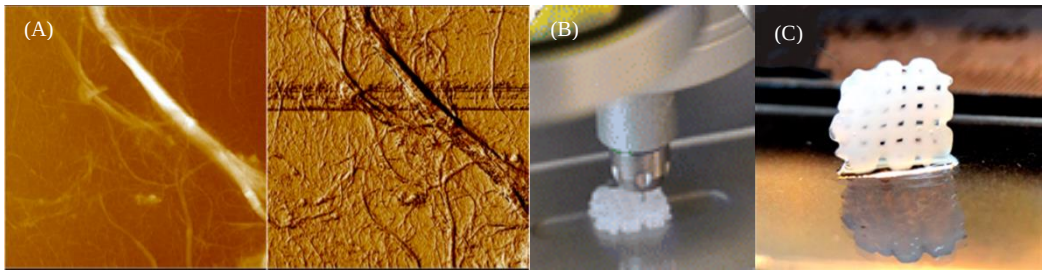

Figure 16 – Example of the use of cellulose nanofibers (NFC) in bioprinting. (A) Atomic force microscopy image of cellulose nanofibers. (B) Bioprinting (C) Alginate + NFC 3D printed grids. (Adapted from Markstedt *et al.*, 2015).[86]

1.3. Aim

As demonstrated in this appraisal, in the past years, the field of bioprinting has evolved at an exorbitant pace, and novel bioinks and optimized bioprinting methods have been developed. Such advancements allowed a successful fabrication of *in vitro* human-scale tissues, an important milestone towards the goal of *in vivo* fully functional organ development. Overall, the 3D bioprinting community has struck major achievements, but there is still plenty of room for improvement. The development of bioinks with adequate mechanical properties and high cell viability, at a reasonable price point, would be a major step forward. Despite the exponential rise in research and development of bioinks, only a limited number of bioinks can match the mechanical,

rheological, and biological pre-requisites in order to be viable post-printing. Additionally, the development of advanced bioprinters with higher resolution and less cost would also be a huge improvement in this research area. In sum, the future of 3D bioprinting and bioinks is highly promising, and this technology can be on the verge of being the leading-edge of medical tissue engineering, as well as on drug testing and diseases investigation.

In this context, the objective of this work is the development of a new natural based hydrogel bioink composed of pectin and cellulose nanofibers for bioprinting of human tissue analogues. These biomaterials were chosen due to their huge potential for 3D bioprinting. Pectin, being one of the main structural polysaccharides of plant cells presents a high biodegradability, and hydrophilicity.[87] Additionally, pectin can form physical hydrogels whenever exposed to divalent cations, such as calcium.[49,87,88] As previously referred cellulose nanofibers have also already demonstrated their potentialities in 3D-bioprinting.[86] However, the combination of pectin and nanocellulose has never been explored in the 3D-bioprinting field. To the best of our knowledge, only one study reported the use of pectin and cellulose nanofibers to produce 3D edible composites for food applications.[89] It is expected that these novel natural based hydrogel bioinks present improved mechanical properties and high cell viability.

2. Materials and Methods

This chapter describes the materials and procedures used to develop a 3D – printable hydrogel-based ink composed of pectin and cellulose nanofibers. It also summarizes the methodologies used to characterize the ink formulations, and the chosen bioprinting procedure. Additionally, there is a brief explanation of the statistical method used to evaluate the flow behavior of the inks.

2.1. Materials

A citrus peel pectin extract (galacturonic acid content ≥ 74.0%) was purchased from Sigma-Aldrich (Sintra, Portugal). Cellulose nanofibers (NFC) suspension was obtained by TEMPO-mediated oxidation and mechanical disintegration of pulp fibers, a methodology that results in NFC with a gel-like consistency (1.86 wt%), with well-individualized nanofibers.[90] Calcium chloride (110.98 g/mol, ≥ 99.9%) was acquired from Sigma-Aldrich (Sintra, Portugal). Ultrapure water (Type 1, 18.2 MΩ◦cm resistivity (at 25 ºC) at 0.5 L min^{-1}) was purified by a Simplicity® Water Purification System (Merck, Darmstadt, Germany).

2.2. Preparation of Pectin solutions, NFC suspensions, Pectin-NFC based inks and corresponding hydrogels

2.2.1. Pectin Solutions

Various pectin solutions (Table 2) were prepared by adding different amounts of pectin extract (1.25, 2.5, 3.75 and 5 g) to 50 mL of ultrapure water, resulting in the following concentrations, 2.5%, 5.0%, 7.5% and 10% (m/v), respectively.

Additionally, 10 g of these pectin solutions were pre-crosslinked with 0.6 g of an aqueous solution of $CaCl_2$ (3% m/v), resulting in pre-crosslinked pectin formulations. The pectin solutions and pre-crosslinked pectin formulations (Table 2) were used for rheological studies. Furthermore, 10 g of a pectin solution with a concentration of 7.5% (m/v), was also pre-crosslinked with different concentrations of $CaCl_2$, namely 0.5%, 0.75%, 1% and 1.5% (m/v), to determine the optimal pre-crosslinking concentration for the 3D-printing assays.

2.2.2. NFC suspensions

NFC suspensions with different concentrations, namely 1% and 10% (m/m) (in respect to the mass of pectin 7.5%), respectively, NFC1 and NFC10, were prepared by dispersing different amounts of NFC gel, in different volumes of ultrapure water, to achieve a final volume of 50 mL, while taking in consideration the amount of water present in the NFC. These suspensions were used for *in-vitro* cytotoxicity assays.

2.2.3. Pectin-NFC based inks and corresponding hydrogels

NFC-reinforced pectin inks (Table 2) were prepared by mixing 3.75 g of pectin extract with variable amounts of NFC (1%, 5%, 10%, and 20% (m/m), in respect to the mass of pectin) Afterwards, the resulting pectin-NFC suspensions, obtained by adding different volumes of ultrapure water (and taking in consideration of the amount of water of the added NFC) to achieve a final volume of 50 mL, were left to homogenize overnight, at room temperature.

Additionally, 0.6 g of a 3% (m/v) aqueous solution of $CaCl_2$ was added drop by drop to 10 g of the suspensions to promote the pre-crosslinking of the inks. To obtain homogenous and bubble-free content inks, all pre-crosslinked inks were placed in a falcon tube and centrifuged (3500 RPM, 2 minutes, 20 ºC). Pre-crosslinked pectin-NFC inks were used for rheological studies and for 3D-printing tests.

Afterwards, the ink samples were submerged in a $CaCl_2$ bath (5 mL, 3% (m/v) of $CaCl_2$), during 48 h. This process led to the complete crosslinking of the inks, resulting in the formation of tight and solid hydrogels. These fully crosslinked hydrogels (Table 2) were used for scanning electron microscopy (SEM), Fourier-transform infrared-attenuated total reflection spectroscopy (FTIR-ATR) and *in-vitro* cytotoxicity assays. For SEM and FTIR-ATR, the hydrogels were previously freeze-dried. For the cytotoxicity assays, hydrogels with a cubic geometry of 1 cm^3 were prepared and, properly sterilized using 3 cycles of UV radiation.

Table 2 summarizes all the samples prepared in this work, including pectin solutions, pectin-NFC suspensions, inks, and fully-crosslinked hydrogels.

Table 2 – Identification and composition of all samples prepared in this study.

Sample Name	Pectin % (m/v)	NFC % (m/m)	Pre-crosslinker % (m/v)
Pectin Solutions			
P2.5	2.5	-	-
P5.0	5.0	-	-
P7.5	7.5	-	-
P10	10	-	-
Pre-crosslinked pectin solutions			
P2.5_CaCl2_3	2.5	-	3.0
P5.0_CaCl2_3	5.0	-	3.0
P7.5_CaCl2_3	7.5	-	3.0
P10_CaCl2_3	10	-	3.0
P7.5_CaCl2_0.5	7.5	-	0.5
P7.5_CaCl2_0.75	7.5	-	0.75
P7.5_CaCl2_1	7.5	-	1.0
P7.5_CaCl2_1.5	7.5	-	1.5
NFC suspensions			
NFC1	-	1.0	-
NFC10	-	10	-
Pectin/NFC suspensions			
P7.5/NFC1	7.5	1.0	-
P7.5/NFC5	7.5	5.0	-
P7.5/NFC10	7.5	10	-
P7.5/NFC20	7.5	20	-
Pre-crosslinked Pectin/NFC suspensions (inks)			
P7.5/NFC1_CaCl2_3	7.5	1.0	3.0
P7.5/NFC5_CaCl2_3	7.5	5.0	3.0
P7.5/NFC10_CaCl2_3	7.5	10	3.0
P7.5/NFC20_CaCl2_3	7.5	20	3.0
P7.5/NFC1_CaCl2_1	7.5	1.0	1.0
P7.5/NFC5_CaCl2_1	7.5	5.0	1.0
P7.5/NFC10_CaCl2_1	7.5	10	1.0
P7.5/NFC20_CaCl2_1	7.5	20	1.0

Pectin/NFC fully-crosslinked hydrogels			
P7.5_CaCl2_3_H	7.5	-	3.0
P7.5/NFC1_CaCl2_3_H	7.5	1.0	3.0
P7.5/NFC5_CaCl2_3_H	7.5	5.0	3.0
P7.5/NFC10_CaCl2_3_H	7.5	10	3.0
P7.5/NFC20_CaCl2_3_H	7.5	20	3.0

2.3. Characterization of the materials

All materials (raw materials, inks, and fully-crosslinked hydrogels) were characterized using different techniques aiming to select the best ink formulation for the printing tests.

2.3.1. Rheology

The rheological characterization of the pectin solutions, pre-crosslinked pectin solutions, pectin-NFC suspensions, and inks (pre-crosslinked pectin-NFC suspensions) was carried out using a *Kinexus Pro* rheometer (Malvern Instruments Limited, Malvern, United Kingdom). Viscosity and shear stress as a function of the shear rate, of the samples, were measured in the range 0,1 – 100 s^{-1} (at least 5 samples per decade), using a cone-plate geometry with a cone angle of 4º, a diameter of 40 mm, and a gap of 1 mm. Additionally, a water lock was used to prevent dehydration of the samples during the measurements. These analyses were carried out at 25 ºC, using a Peltier module for temperature control.

2.3.2. Scanning Electron Microscopy (SEM)

The morphology of the fully crosslinked hydrogels was assessed by scanning electron microscopy (SEM). The samples were freeze-dried prior to the visualization. A SEM *Hitachi SU-70* equipment (Hitachi High-Technologies Corporation, Tokyo, Japan) operated at 4 kV, was used to obtain surface and cross-sectional micrographs. The samples were previously coated with a carbon film. The dimension of the pores was determined by analysis of the cross-section images, using the ImageJ (at least, 10 pores were analysed in each case).

2.3.3. Fourier transform infrared-attenuated total reflection (FTIR – ATR)

The FTIR-ATR spectra of the fully crosslinked hydrogels were acquired in a *Perkin Elmer FT-IR System Spectrum BX spectrophotometer* (Perkin-Elmer, Waltham, MA, USA), equipped with a single horizontal *Golden Gate ATR* cell. The scans were performed in the range of 4000-500 cm^{-1} at a resolution of 4 cm^{-1} with an interval of 1 cm^{-1}. The samples were freeze-dried prior to the analysis.

2.4. *In-vitro* Cytotoxicity Assay

The cytotoxicity of the fully-crosslinked hydrogels (P7.5_CaCl2_3_H, P7.5/NFC1_CaCl2_3_H, P7.5/NFC10_CaCl2_3_H) and NFC suspensions with different concentrations (NFC1 and NFC10), for comparison purposes, were evaluated in a human keratinocyte cell line (HaCaT cells) by using the 3-(4,5-dimethylthiazol-2-yl)-2,5-diphenyl tetrazolium bromide (MTT) assay. These cells were grown in complete Dulbecco's modified eagle medium (DMEM) supplemented with 10% FBS, 2 mM L-glutamine, 10,000 U mL^{-1} penicillin/streptomycin, and 250 µg mL^{-1} fungizone, at 37 ºC, in 5% CO_2 humidified atmosphere. The cells were observed daily in an inverted-phase-contrast *Eclipse TS100 microscope* (Nikon, Tokyo, Japan). The tests were performed for Pectin (P7.5_CaCl2_3_H), Pectin + NFC 1% (P7.5/NFC1_CaCl2_3_H), and Pectin + NFC 10% (P7.5/NFC10_CaCl2_3_H), and as a negative control, HaCaT cells were treated identically, as described for the samples, but exposed only to DMEM medium.

Hydrogel samples with 1 x 1 x 1 cm^3 were prepared, sterilized using 3 cycles of ultraviolet (UV) radiation, and then, promptly, incubated with 5 mL of DMEM medium at 37 ºC, with 5% CO_2, for 24 h in order to prepare the sample extract. HaCaT cells were seeded in a 96-well plate configuration with a total of 6000, 4000, and 2000 cells per well. The number of cells seeded in each well depends on the length of the determined assay, being 6000 cells for a 24 h assay, 4000 for 48 h, and 2000 for 72 h. Later, these cells were exposed to extracts of P7.5_CaCl2_3_H, P7.5/NFC1_CaCl2_3_H, P7.5/NFC10_CaCl2_3_H, NFC1, and NFC10 for the duration of each assay (24, 48 and 72 h). These extracts were obtained from the previously incubated samples, with a minimum of 5 replicates/wells per sample. After that, 50 µL of MTT (1 g L^{-1}) was added to each well and incubated for 4 h, at 37 ºC, in a 5% CO_2 humidified atmosphere. Afterwards, the culture medium with MTT was removed and replaced by 150 µL of dimethyl sulfoxide (DMSO), and finally, the plate was placed in an orbital shaker for 2 h, in a dark environment, to completely dissolve the formazan

crystals. The absorbance of the samples was measured with a *BioTek Synergy HT plate reader* (Synergy HT Multi-Mode, BioTeK, Winooski, VT, USA) at 570 nm, with blank corrections. The cell viability was calculated concerning the control cells:

$$Cell\ viability\ (\%) = \left[\frac{(Abs_{sample} - Abs_{DMSO})}{(Abs_{control} - Abs_{DMSO})}\right] * 100$$

Where Abs_{sample} is the absorbance of the sample, Abs_{DMSO} is the absorbance of the solvent (DMSO) and $Abs_{control}$ is the absorbance of the control.

2.5. Printing assays

2.5.1. Optimization of the 3D printing parameters

The printing assays were performed using a commercially available 3D printer, *3D Bioplotter® Developer Series* (EnvisionTEC, Germany), represented in Figure 17. Three factors were optimized during the experimental assays: pressure, velocity, and nozzle diameter. It was used a 3D model of a 30x30 box with a layer height of 320 μm or 100 μm and a distance between lines of 2.5 mm or 1.5 mm (shown in Figure 18 as "x"), designed using a CAD software.

Figure 17 – 3D Bioplotter® Developer Series (EnvisionTEC, Germany). (Obtained from envisiontec.com)

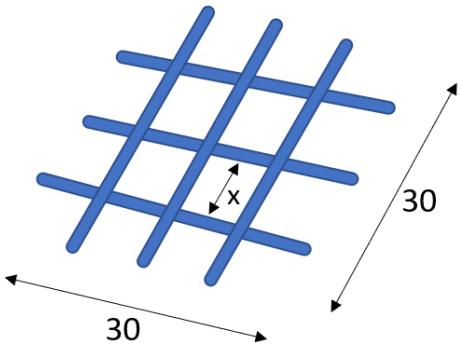

Figure 18 – 3D blueprint designed with CAD software with 30x30 mm with a spacing of 1.5 to 2.5 mm between lines (Represented as "x").

After the characterization of the inks, the sample with a pectin concentration of 7.5% (m/v), P7.5, was selected for the first optimization tests. Before 3D printing, some printing parameters must be optimized, namely, optimal pressure, velocity, and nozzle diameter. These optimization assays consist in printing filaments of ink using different combinations of pressure (1.0, 1.5, 2.0, 2.5, 3.0 bar), velocity (5.0, 7.5, 10.0, 12.5, 15.0 mm/s), and nozzle diameter (0.20, 0.25, 0.41 mm), in order to determine the optimal parameter combination for printing. The P7.5 solution was tested with several $CaCl_2$ concentrations, namely, 0.5%, 0.75%, 1%, 1.5% (m/v) and the optimal printing parameters are defined in Table 4. Afterwards, the selected Pectin-NFC inks, P7.5/NFC1_CaCl2_1 and P7.5/NFC10_CaCl2_1 were printed using the previously determined parameters.

2.6.Statistical Analysis

The Herschel-Bulkley's model (OriginPro, version 2021, OriginLab Corporation, Northampton, MA, USA) was used to define the flow behavior of the inks. Newton's law of viscosity claims that for a wide range of fluids, their viscosity is not proportional to the shear rate applied. Fluids that obey this law are called Newtonian fluids. However, there are fluids in which the viscosity is dependent on shear rate, these are called Non-Newtonian fluids (Figure 19). Non-newtonian fluids are widely diverse and can be characterized as shear thickening/dilatant, shear-thinning/pseudoplastic, thixotropic, and viscoplastic fluids.[91]

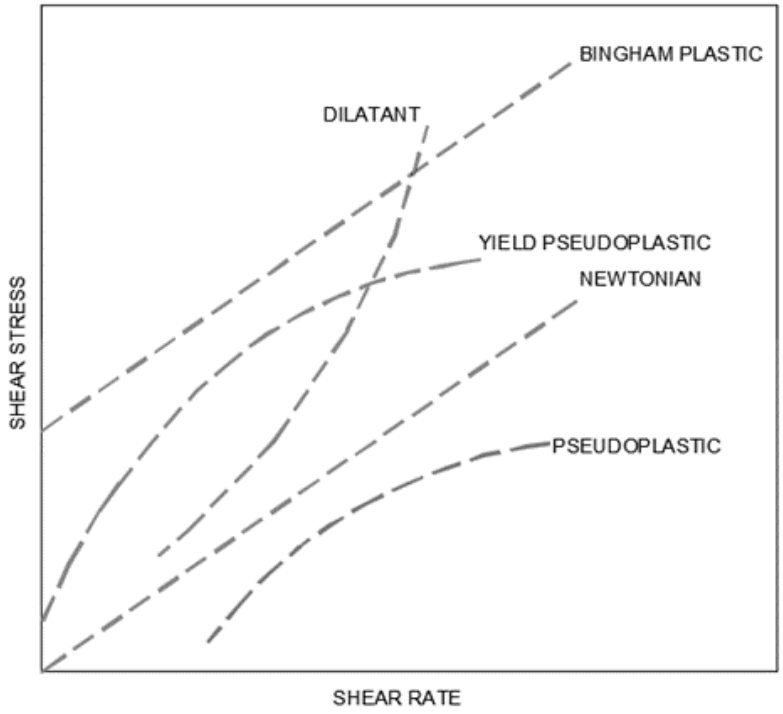

Figure 19 – Types of fluids with shear stress as a function of shear rate.

The Herschel-Bulkley model, a common mathematical model used to describe fluids with nonlinear/non-Newtonian behavior, was used to fit the flow curves of the inks developed in this study, by using the following equation:

$$\tau = \tau_0 + K * \gamma^n$$

Where τ is the shear stress (Pa), τ_0 the yield shear stress (Pa), K the consistency factor (Pa ◦ s^n), γ represents the shear rate (s^{-1}) and n is the flow behavior index. The regression analysis had the objective of calculating the τ_0, K and n of each sample.

The Herschel-Bulkley model defines each fluid using the following conditions: [91,92]

τ_0 = 0 and n = 1 → Newtonian behavior,

τ_0 > 0 and n = 1 → Bingham plastic behavior,

τ_0 = 0 and n < 1 → Pseudoplastic/shear-thinning behavior,

τ_0 = 0 and n > 1 → Dilatant/Shear-thickening behavior,

τ_0 > 1 and n < 1 → Yield pseudoplastic behavior.

3.Results and Discussion

The present work aimed to develop hydrogel-based pectin-NFC bioinks for application in 3D-bioprinting. In this perspective, inks with different NFC contents were obtained by mixing pectin extract with a NFC suspension in distinct proportions, followed by a pre-crosslinking step with a $CaCl_2$ solution. To achieve this goal, firstly, several pectin solutions were characterized in terms of shear viscosity and shear stress as a function of shear rate. The pectin solution with better rheological properties, for printing purposes, was then combined with different amounts of NFC yielding a set of pectin-NFC suspensions with different NFC contents. These suspensions were, finally, pre-crosslinked to adjust the rheological properties of the inks envisioning their 3D-printing. All pectin solutions, NFC-pectin suspensions, and pre-crosslinked inks were characterized in terms of their rheologic behavior to select the best pectin-NFC combination for the optimization of the 3D-printing assays. Finally, the optimization of the 3D-printing process of these inks was carried out, where the optimal pressure, velocity, nozzle diameter, and printed layers were defined. Additionally, fully-crosslinked hydrogels were also characterized for their chemical composition (FTIR-ATR spectroscopy), morphology (SEM), and *in-vitro* cytotoxicity.

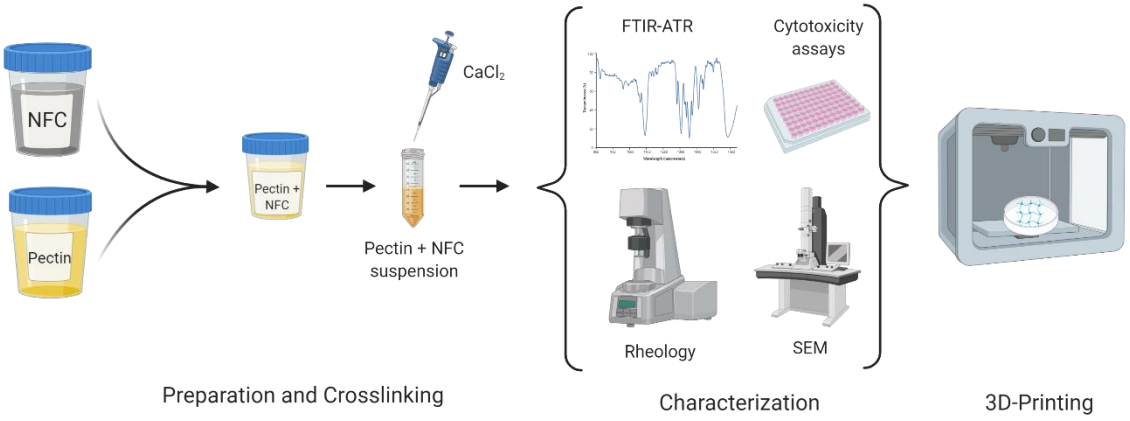

Figure 20 - Schematic representation of the chosen procedure to prepare, characterize and obtain 3D printed hydrogels. (Created with BioRender.com)

3.1. Rheological characterization

The rheological characterization aims to study how the materials react to a certain stress,[91] and therefore comprehend how the inks will behave during a 3D-printing assay. In this sense, several rheological studies were conducted (all at a

controlled temperature of 25 ºC) to determine the most desirable concentrations of pectin, crosslinking agent and NFC.

3.1.1. Pectin solutions

As previously mentioned, pectin solutions with different concentrations, namely 2.5, 5, 7.5 and 10% (m/v) (Table 2) were prepared aiming to determine the optimal pectin concentration to further carry out the preparation of the pectin-NFC suspensions. The four pectin solutions, P2.5, P5.0, P7.5, and P10, were characterized in terms of their viscosity and shear stress. The results are presented in Figure 21.

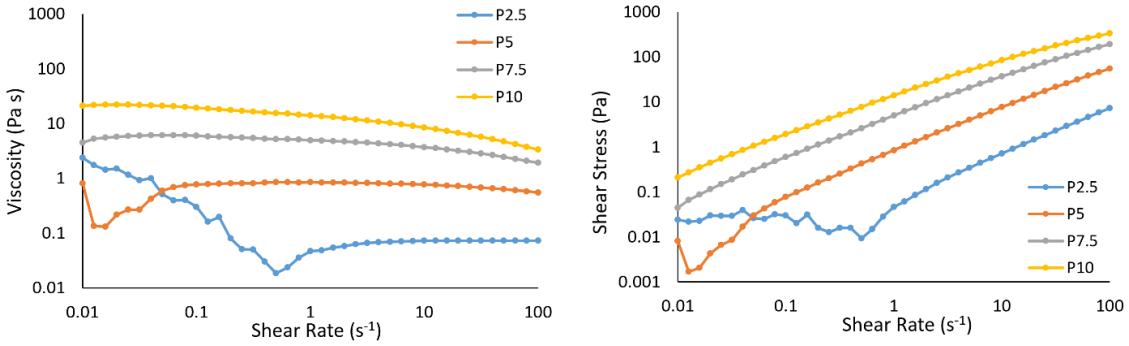

Figure 21 - Viscosity (left) and shear stress (right) measured as a function of shear rate for pectin solutions with different concentrations.

As expected, the viscosity and shear stress of the pectin solutions increases with the increase of the concentration of pectin.[93] Additionally, all pectin solutions present a shear-thinning behavior, which is defined by the decrease in viscosity as the shear rate increases, a feature that improves the overall printability, leading to a higher printing fidelity and, potentially, higher post-printing cell viability.[13,94]

In order to determine the influence of a pre-crosslinking step on the rheological properties of the solutions, the different pectin solutions were pre-crosslinked with a 3% (m/v) $CaCl_2$, and the viscosity and shear stress measured also as a function of shear rate (Figure 22).

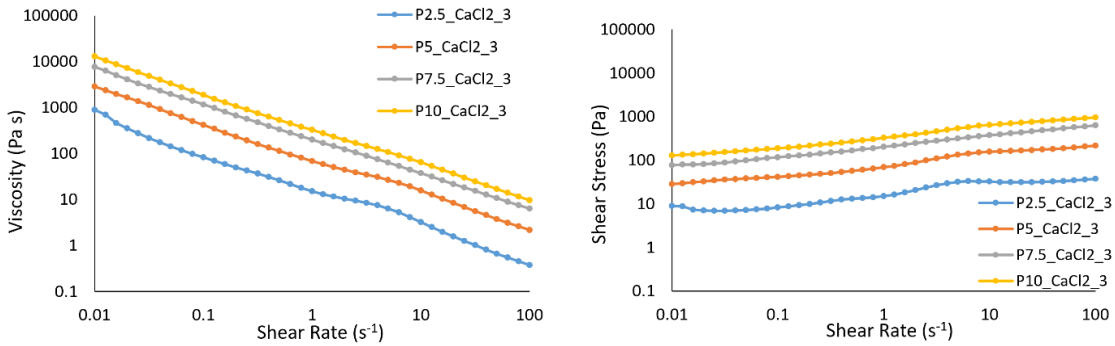

Figure 22 - Viscosity and shear stress measured as a function of shear rate of pre-crosslinked (3% $CaCl_2$) pectin solutions with different pectin concentrations.

As previously observed for the pectin solutions, the viscosity and shear stress of the pre-crosslinked pectin solutions also increases with the concentration of pectin. However, these values are noticeably higher, over three levels of magnitude, than those obtained for the non-pre-crosslinked pectin solutions (Figure 21). This behavior is similar to what has been reported in literature for a pectin methacrylate solution, for which by adding 5 mM of $CaCl_2$, an increase of over three levels of magnitude in the viscosity was also observed.[87,88] This behavior is due to the crosslinking mechanism with $CaCl_2$, as it links the chains of pectin, leading to the formation of a hydrogel.[87] Additionally, all pre-crosslinked pectin formulations also show a shear-thinning behavior similarly to the pectin solutions.

Considering the desirable viscosity ($0.03 – 6 \times 10^4$ Pa s)[95] of ink formulations for extrusion bioprinting applications in the printing range ($1 – 100\ s^{-1}$)[96] and the results obtained in the rheological characterization of the pectin solutions with different concentrations, the pectin solution with 7.5% (m/v) concentration, namely P7.5, was selected for the incorporation of NFC due to its set of properties.

3.1.2. Pectin-NFC suspensions and inks

After selecting the best pectin concentration, different amounts of NFC were added to this pectin solution aiming to prepare pectin-NFC formulations with different NFC amounts, specifically 1, 5, 10 and 20% (m/m). Then, the rheological properties of these suspensions were investigated to select the optimal formulation composition for 3D-bioprinting.

The first assays involved the measurement of the shear viscosity and shear stress, as a function of shear rate, of the different pectin-NFC suspensions. These results are shown in Figure 23.

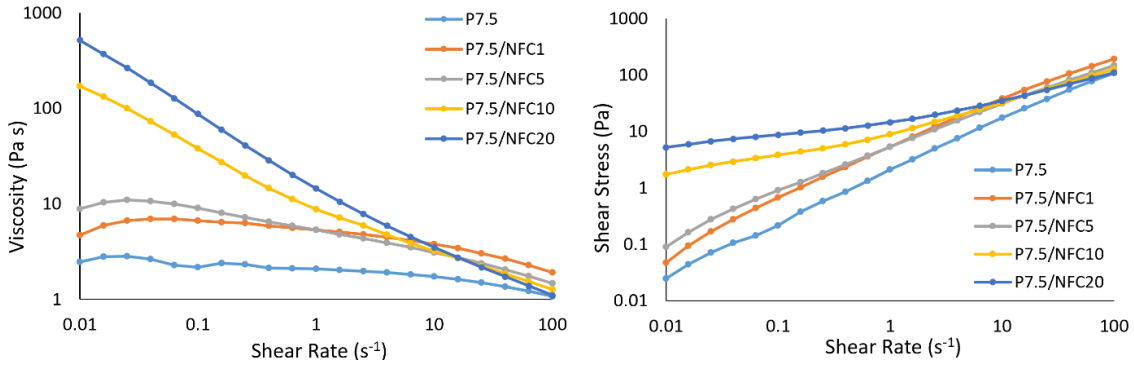

Figure 23 - Viscosity and shear stress as a function of shear rate of different concentrations of Pectin-NFC suspensions.

As expected, the viscosity and shear stress of the pectin-NFC suspensions increase with the content of NFC, and all formulations present a shear thinning behavior. Similar results have also been reported for alginate-NFC based inks.[86]

Additionally, a batch of pre-crosslinked ($CaCl_2$ 3% (m/v)) pectin-NFC suspensions (inks) were prepared and tested, to assess the influence of a pre-crosslinking stage in the viscosity and shear stress of the pectin-NFC based inks. The results are shown in Figure 24.

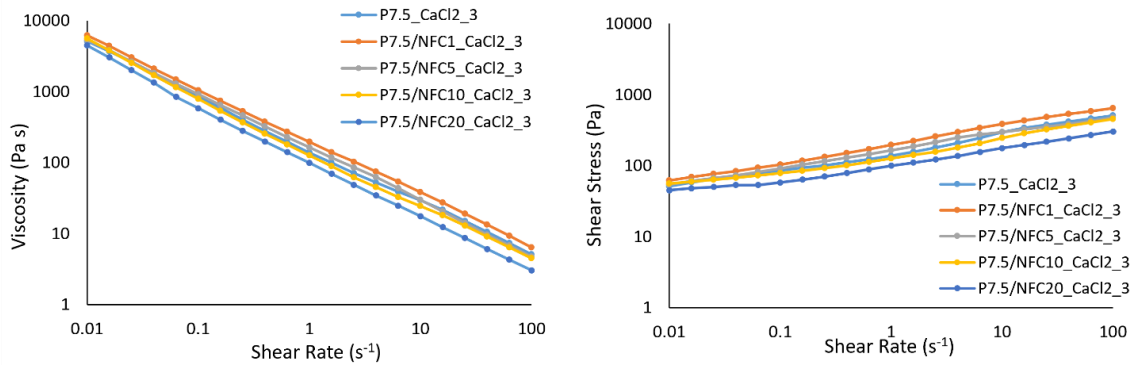

Figure 24 - Viscosity (left) and shear stress (right) as a function of shear rate of different concentrations of pre-crosslinked (3% m/v $CaCl_2$) Pectin-NFC suspensions (inks).

All pectin-NFC inks show a decrease of viscosity as the shear rate increases (Figure 24), further confirming the highly desirable shear-thinning behavior.[74] However, the main conclusion taken from these tests is that independently of the

content of NFC the viscosity and shear stress of the different samples is very similar between them. Moreover, the values of shear viscosity and shear stress are over three levels of magnitude higher than those of pectin-NFC suspensions (Figure 23). These results are a clear indication that the pre-crosslinking has a stronger effect on the rheological behavior of the inks than the addition of NFC. These results are in accordance with what was previously reported in the literature for alginate-NFC inks pre-crosslinked with calcium carbonate ($CaCO_3$).[97]

However, preliminary printing assays revealed that none of these ink formulations were able to be printed at an acceptable pressure and velocity because of their high viscosity in the extrusion 3-D printing range of 1 to 100 s^{-1}.[96] Due to this, lower crosslinking concentrations were tested (0.5, 0.75, 1, 1.5 % (m/v)), and a $CaCl_2$ concentration of 1% (m/v) was found to be an adequate concentration for printing. So, the following rheological results (Figure 25) take in regard the pre-crosslinked pectin-NFC inks with a lower concentration of $CaCl_2$ (1% (m/v)) to confirm their behavior and suitability for 3D-printing.

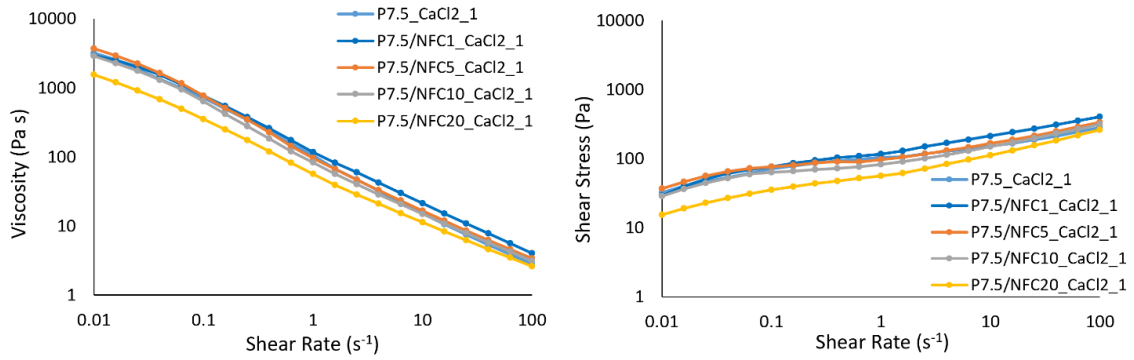

Figure 25 - Viscosity (left) and shear stress (right) measured as a function of shear rate of different concentrations of pre-crosslinked (1% m/v $CaCl_2$) Pectin-NFC suspensions (inks).

The formulations pre-crosslinked with 1% (m/v) $CaCl_2$ also presented a shear-thinning behavior, as previously observed for the inks prepared with a higher concentration of $CaCl_2$ (3% (m/v)). As expected, the viscosity and shear stress values, between 1 to 100 s^{-1} (shear rate extrusion printing range),[96] of these 1% inks are much lower, making them certainly 3D printable and more likely to harvest a higher post-printing cell viability.[98]

Aiming to confirm and further study the flow behavior of the samples, the results of the rheological characterization were fitted to the Herschel-Bulkley model (Table 3). These results confirm the highly favorable shear thinning/pseudoplastic behavior of most of the samples investigated. However, only three samples, namely P7.5, P7.5/NFC1, and P7.5/NFC5, demonstrate a normal pseudoplastic behavior ($\tau_0 = 0$ and $n < 1$). The remaining samples show a yield pseudoplastic behavior, which is characterized by the need of surpassing a force threshold (τ_0) to begin extruding a formulation.[89]

The values of τ_0 for the samples P7.5/NFC1_CaCl2_3 and P7.5/NFC5_CaCl2_3 are, 0 ± 16.34 and 0 ± 12.29, respectively, which could lead to a misinterpretation. Following the Herschel-Bulkley model, P7.5/NFC1_CaCl2_3 and P7.5/NFC5_CaCl2_3 present a normal shear-thinning fluid behavior ($\tau_0 = 0$ and $n < 1$), contrarily to the remaining pre-crosslinked samples. However, in the Figure 24, all pre-crosslinked samples present a similar flow behavior, yield pseudoplastic. Considering this, and the fact that the values from the Herschel-Bulkley model are presented with such uncertainty (high error values), the behavior of these samples was defined as yield pseudoplastic.

Moreover, it is also observable that the inks (pre-crosslinked formulations) attain a more defined pseudoplastic behavior whenever compared to their suspension counterparts (lower flow behavior index (n) represents a more defined pseudoplastic behavior)[99] due to the effect of the crosslinking treatment. However, as already stated, the samples crosslinked with 1% (m/v) $CaCl_2$ (Figure 25) present considerably lower viscosities than those crosslinked with 3% $CaCl_2$ (m/v) (Figure 24). As an example, when comparing the samples P7.5/NFC10_CaCl2_3 (102.61 ± 6.47 Pa ◦ s^n) and P7.5/NFC10_CaCl2_1 (48.25 ± 3.88 Pa ◦ s^n) it is observable a two-fold decrease in viscosity.

For the pectin-NFC inks, the values of the consistency factor (K) decrease as the NFC concentration increases, which seems to be contradictory to what is reported in the literature.[89] However, in the literature the samples are exposed to a full crosslinking procedure prior to the rheological assays, while in this work only a pre-crosslink (reduced quantity) is applied. Additionally, higher concentrations of NFC can interfere with the crosslinking of pectin, resulting in a less stiff hydrogel, and consequently a lower consistency factor value.

Table 3 – Rheological properties of the pectin solution, pectin-NFC suspensions and ink formulations using the Hershel-Bulkley model. R^2 = Regression coefficient.

Sample	τ_0	K (Pa ◦ s^n)	n	R^2
P7.5	0 ± 0.32	3.18 ± 0.18	0.76 ± 0.01	0.998
P7.5/NFC1	0 ± 0.86	8.43 ± 0.59	0.68 ± 0.02	0.998
P7.5/NFC5	0 ± 0.41	6.61 ± 0.29	0.67 ± 0.01	0.999
P7.5/NFC10	1.57 ± 0.14	7.59 ± 0.12	0.61 ± 0.003	0.999
P7.5/NFC20	5.90 ± 0.21	8.24 ± 0.19	0.55 ± 0.01	0.999
P7.5_CaCl2_3	8.44 ± 11.1	142.21 ± 12.64	0.28 ± 0.02	0.992
P7.5/NFC1_CaCl2_3	0 ± 16.34	211.69 ± 18.48	0.25 ± 0.01	0.994
P7.5/NFC5_CaCl2_3	0 ± 12.29	167.34 ± 13.79	0.23 ± 0.01	0.995
P7.5/NFC10_CaCl2_3	28.05 ± 5.69	102.61 ± 6.47	0.31 ± 0.01	0.996
P7.5/NFC20_CaCl2_3	17.35 ± 2.92	82.45 ± 3.32	0.35 ± 0.01	0.998
P7.5_CaCl2_1	24.10 ± 8.74	73.98 ± 9.91	0.26 ± 0.02	0.986
P7.5/NFC1_CaCl2_1	15.41 ± 5.73	104.99 ± 6.51	0.28 ± 0.01	0.996
P7.5/NFC5_CaCl2_1	46.17 ± 4.48	51.78 ± 5.00	0.37 ± 0.02	0.992
P7.5/NFC10_CaCl2_1	35.13 ± 3.49	48.25 ± 3.88	0.38 ± 0.01	0.994
P7.5/NFC20_CaCl2_1	16.02 ± 1.82	39.67 ± 2.01	0.39 ± 0.01	0.998

3.2.FTIR-ATR analysis

Following the rheological characterization of the pectin solutions, pectin-NFC suspensions and inks, the corresponding fully crosslinked hydrogels were obtained by submerging the selected pectin solution and the pectin-NFC suspensions in a $CaCl_2$ bath (5 mL, 3% (m/v) of $CaCl_2$), for 48 h. These hydrogels were freeze-dried, and their structural characterization was carried out by FTIR-ATR, as depicted in Figure 26. Pure NFC was also analysed for comparison purposes. By using this spectroscopic technique, we can confirm the presence of the most functional groups of NFC and pectin and if any interactions were established.

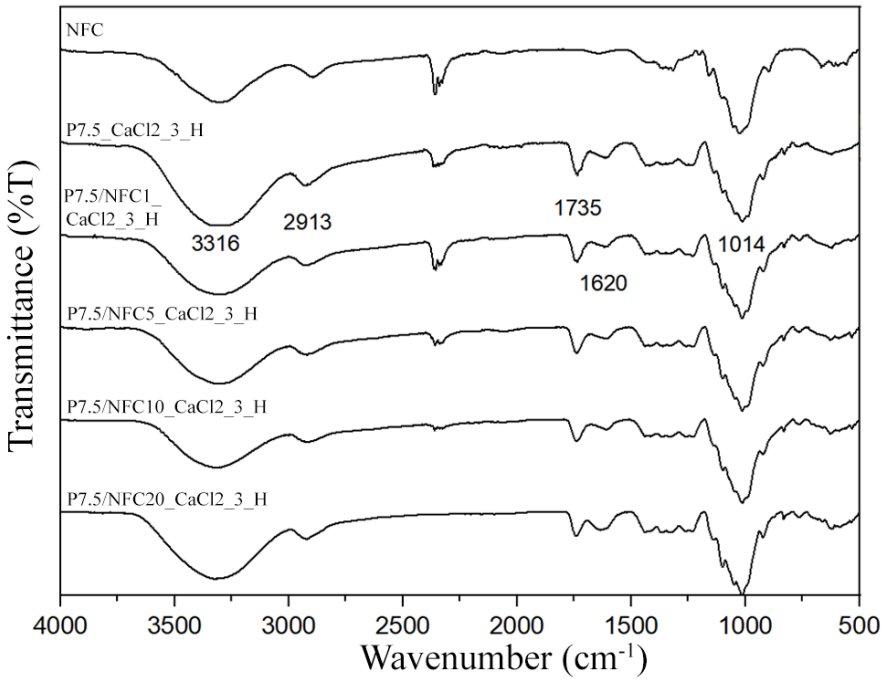

Figure 26 – FTIR-ATR spectra of the pectin-NFC hydrogels with different NFC contents.

The spectrum of the pure pectin hydrogel (P7.5_CaCl2_3_H) displays the expected absorption bands of pectin, namely at 3316 cm^{-1} (O-H stretching), 2913 cm^{-1} (C-H stretching), 1735 cm^{-1} (C = O stretching), 1620 cm^{-1} (deformation of O-H) and 1014 cm^{-1} (stretching of C-O).[100–102]

The spectrum of pure NFC shows the typical absorption bands of a cellulosic substrate, viz. 3316 cm^{-1} (O-H stretching),[100] 2913 cm^{-1} (C-H stretching),[101,102] 1620 cm^{-1} (O-H deformation) and 1014 cm^{-1} (C–O stretching).

As expected, the spectra of the P7.5/NFC1_CaCl2_3_H, P7.5/NFC5_CaCl2_3_H, P7.5/NFC10_CaCl2_3_H, and P7.5/NFC20_CaCl2_3_H hydrogels are a perfect combination of the spectra of pectin and NFC. Moreover, no displacements of bands were observed suggesting that the interaction between NFC and pectin are moderate.[103]

3.3.Scanning Electron Microscopy (SEM)

SEM analysis of the pectin-NFC hydrogels were carried out to analyze their morphological features, since the porosity is an important parameter for the desired applications, namely cell proliferation in tissue regeneration.[104] Surface and cross-section images of the freeze-dried hydrogels are presented in Figure 27.

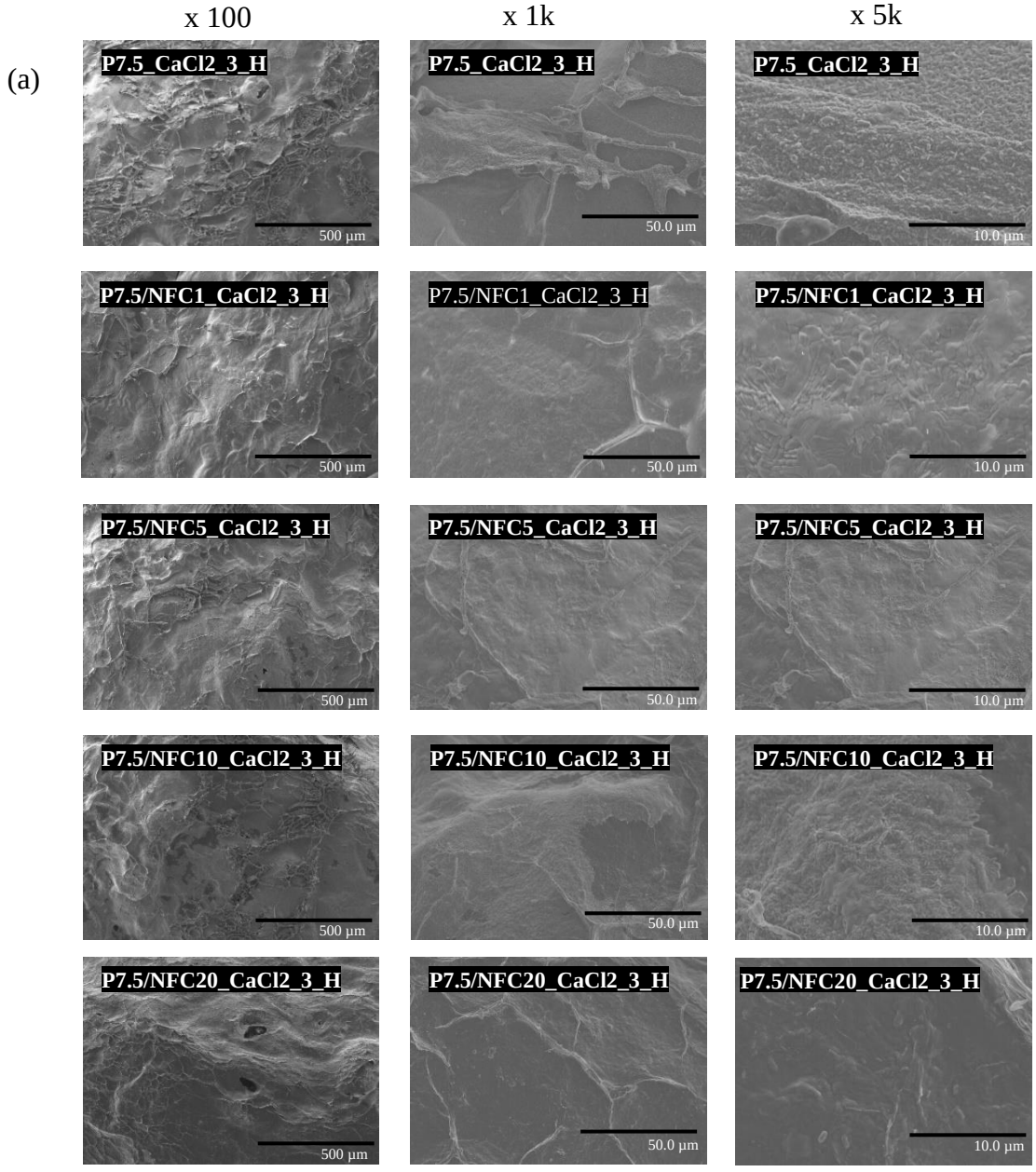

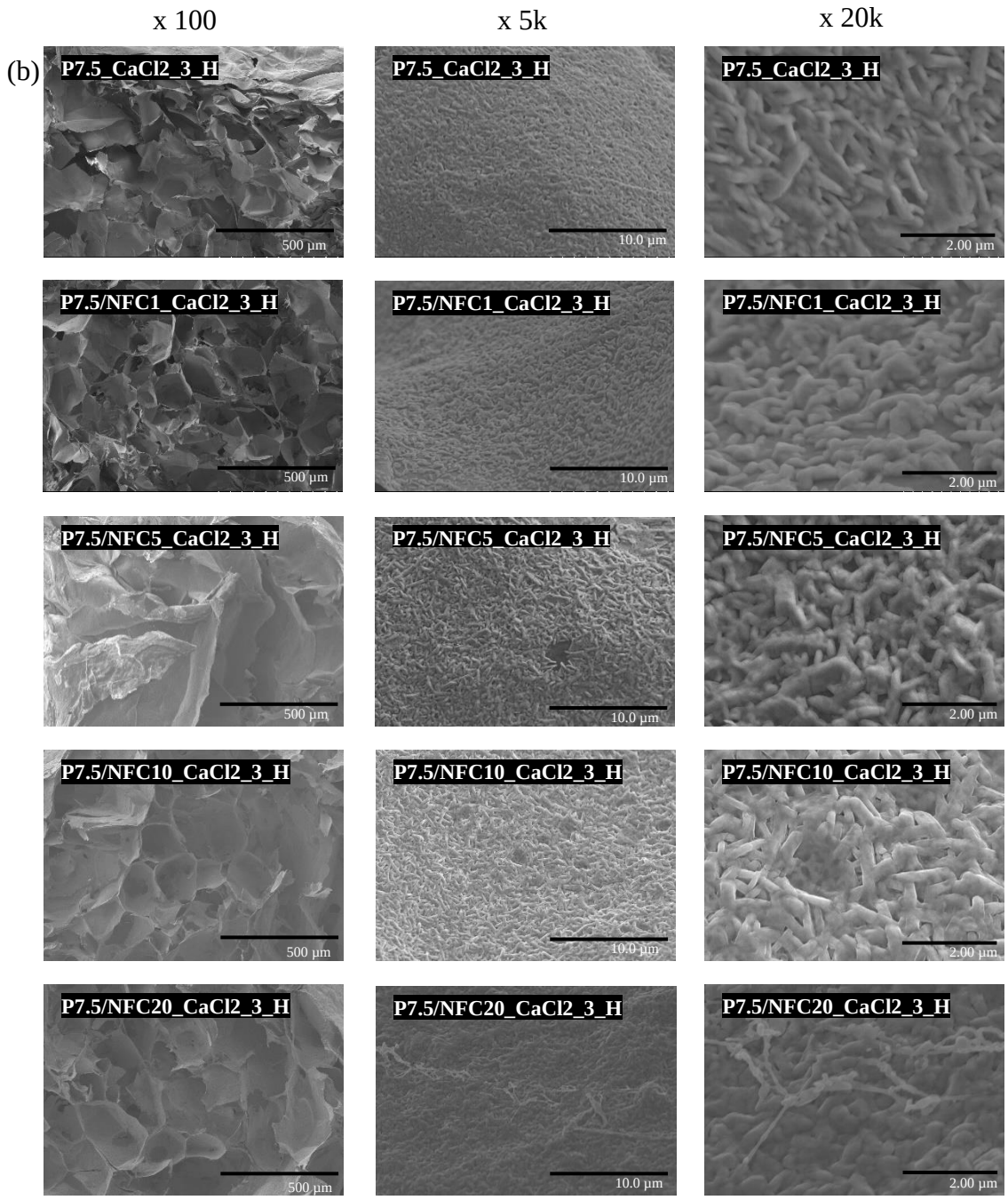

Figure 27 – Scanning electron microscopy (SEM) micrographs of the surface (a) and cross-section (b) of P7.5_CaCl2_3_H, P7.5/NFC1_CaCl2_3_H, P7.5/NFC5_CaCL2_3_H, P7.5/NFC10_CaCl2_3_H, and P7.5/NFC20_CaCl2_3_H.

Regarding the surface micrographs (Figure 27a), all samples revealed a rough surface, similarly to that reported in the literature for other pectin samples.[105] No major differences were noted between samples, except for the samples with higher NFC contents, where cellulose nanofibers are more visible. In the cross-section micrographs (Figure 27b), it is clearly perceptible that these hydrogels have a porous structure, with

similar pore size for all samples (pore dimension of 155.0 ± 35.7 µm), as seen in the micrographs with a magnification of x100. As for the cellulose nanofibers, they can only be observable in the samples with higher NFC contents, in particular for the cross-section sample P7.5/NFC20_CaCl2_3_H, with several strands that can be seen at x5k and x20k magnifications.

In sum, the SEM micrographs confirmed that the pectin-NFC hydrogels have an adequate morphology and topology for tissue regeneration applications, with a multitude of pores that are essential for cell adhesion and proliferation.[104]

3.4. *In-vitro* cytotoxicity assay

The cytotoxicity of the pectin-NFC hydrogels, namely, P7.5/NFC1_CaCl2_3_H and P7.5/NFC10_CaCl2_3_H, and of their individual components, P7.5_CaCl2_3_H, NFC1 and NFC10, for comparison purposes, was investigated towards HaCaT cells in order to confirm the hydrogel suitability for cell laden. The results are shown in Figure 28.

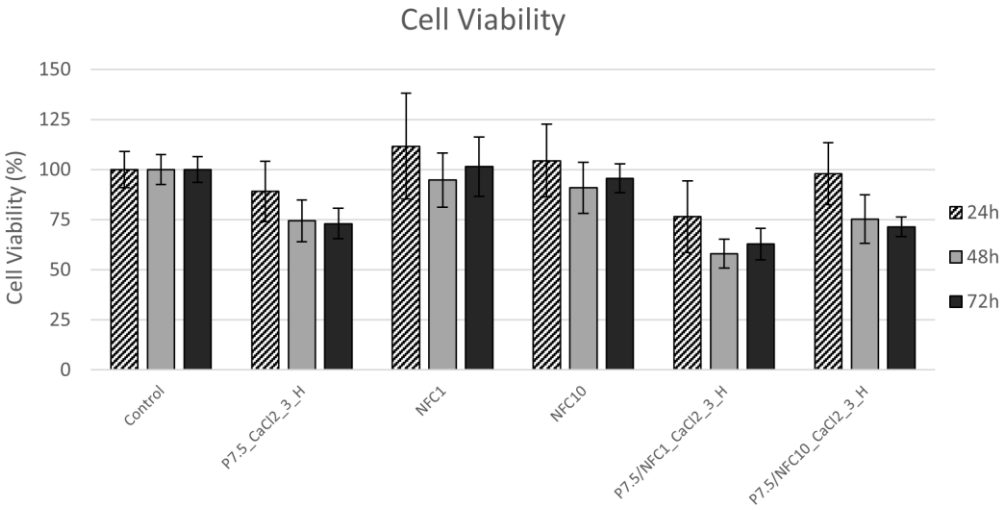

Figure 28 – HaCaT cells viability after exposure to P7.5_CaCl2_3_H, NFC1, NFC10, P7.5/NFC1_CaCl2_3_H and P7.5/NFC10_CaCl2_3_H for 24, 48, and 72 h (2 assays with a minimum of 5 replicas per sample).

The results displayed in Figure 28, confirm that pure pectin and NFC are non-cytotoxic towards HaCaT cells, since the cell viabilities for the samples P7.5_CaCl2_3_H, NFC1 and NFC10 surpass the threshold of 70%, confirming their potential for clinical use.[106] Pectin (P7.5_CaCl2_3_H) reported higher values at 24 h

with 89 ± 14% of cell viability, while for 48 h and 72 h a slight decrease was observed, with similar values, 74 ± 10% and 73 ± 7%, respectively. A previous study reported a dose-dependent cytotoxicity effect with pectin concentrations up to 0.075% (0.00075 g/mL) towards HaCaT cells, reaching values as low as 62.54% of cell viability.[107] However, in this study by using a higher pectin concentration of 7.5 % (m/v) viz. 0.075 g/mL, higher values of cell viability were obtained.

On the other hand, the NFC-based suspensions showed cell viability values in the order of 100%. NFC1 reported higher values in the 24 h and 72 h assays with 111 ± 26% and 101 ± 14% cell viabilities, respectively. For 48 h a slight decrease was observed with a mean of 94 ± 13% cell viability. The sample NFC10, followed the same trend, demonstrating slightly lower cell viabilities at 48 h and 72 h, but with values also close to 100% cell viability. These values confirm the non-cytotoxic behavior of NFC towards HaCaT cells, as reported in the literature for other cell lines, as cardiac myoblast cells and fibroblasts.[86,108]

Regarding the pectin-NFC hydrogels (P7.5/NFC1_CaCl2_3_H and P7.5/NFC10_CaCl2_3_H), the cell viabilities are lower than those of the individual components. According to figure 28, the only cytotoxic sample is the P7.5/NFC1_CaCl2_3_H hydrogel which at 48 h has a cell viability of only 58%. However, the hydrogel with the highest content of NFC, P7.5/NFC10_CaCl2_3_H, showed a higher cell viability (Figure 28). In fact, other studies involving the combination of NFC with other natural polymers, namely alginate, revealed non-citotoxicity towards a fibroblast cell line, which goes in agreement with our results.[86] We believe that this lower cell viability for the sample P7.5/NFC1_CaCl2_3_H is due to a contamination because all the other samples, even the pure pectin hydrogel, are not cytotoxic. However, further studies will be required to clarify this behavior.

3.5. Optimization of the 3D-printing conditions

The optimization of the 3D-printing conditions was carried out for the pre-crosslinked inks prepared, and several printing parameters were tested, namely nozzle diameter, dispensing pressure, and printing velocity. These tests consisted in printing ink filaments using different combinations of nozzle diameter, pressure and velocity. The optimal concentration of the $CaCl_2$ solution for the pre-crosslinking of the pectin-based inks was also confirmed aiming to obtain 3D-bioprintable inks, so several pectin solutions were crosslinked with different amounts of $CaCl_2$, 0.5, 0.75, 1 and 1.5%

(m/v), yielding samples P7.5_CaCl2_0.5, P7.5_CaCl2_0.75, P7.5_CaCl2_1, P7.5_CaCl2_1.5, respectively (Table 4).

In what respects to the nozzle diameter, three different diameters were tested (0.20 mm, 0.25 mm and 0.41 mm), for all pectin samples pre-crosslinked with different amounts of calcium chloride, and the printing results for sample P7.5_CaCl2_1 are shown in Figure 29 as an example. The use of a nozzle diameter of 0.41 mm was discarded due to the high amount of ink deposited leading to a lack of printing resolution. A diameter of 0.20 mm, despite being the highest resolution nozzle, was also rejected since it is too narrow, possibly endangering the viability of the cells.[109,110] Considering this, a nozzle diameter of 0.25 mm was selected as it presents the best resolution (Table 4 and Figure 29).

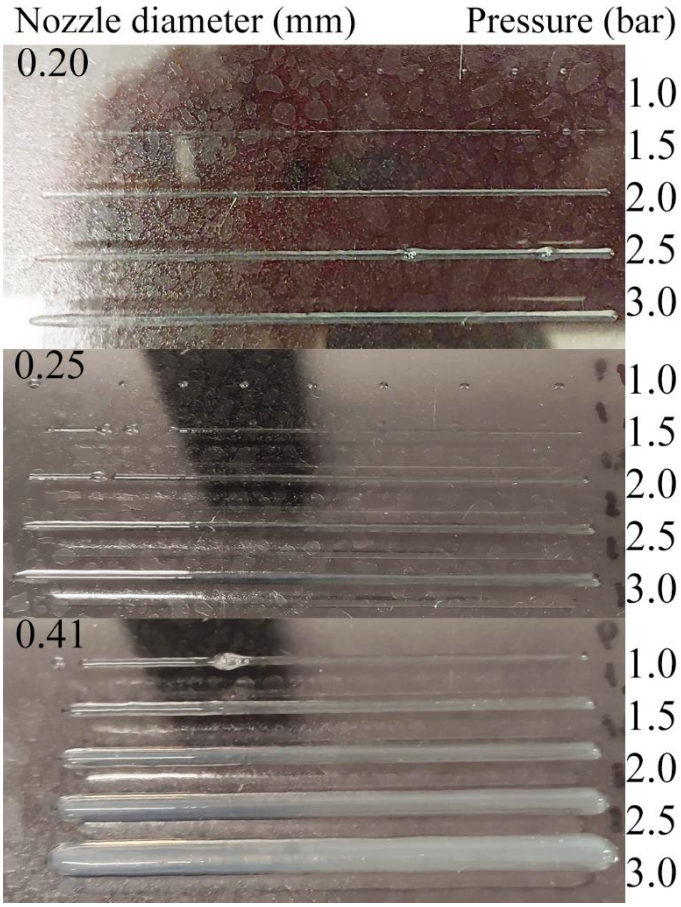

Figure 29 – Printing studies of P7.5_CaCl2_1 using different nozzle diameters and pressures. From top to bottom, printing results with a nozzle diameter of 0.20 mm, 0.25 mm, and 0.41 mm, and using a fixed printing speed of 7.5 mm/s and variable pressures, namely 1, 1.5, 2, 2.5 and 3 bar.

However, of all parameters, dispensing pressure is the one with the highest effect on cell viability,[111] so an equilibrium had to be considered between dispensing pressure and printing velocity in order to maintain the necessary printing resolution without damaging the cells. So, and according to the literature, a pressure of 2 bar was chosen, since it allows a balance between cell viability, printing velocity of 7.5 mm/s and printing resolution.[109]

All samples were exposed to identical combinations of nozzle diameter (0.20, 0.25 and 0.41 mm), dispensing pressure (1.0, 1.5, 2.0, 2.5, 3.0 bar) and printing velocity (5.0, 7.5, 10.0, 12.5, 15.0 mm/s), a summary of the optimal printing parameters tested for each ink is present in Table 4.

Table 4 – Pectin printability optimization assays. Ø = nozzle diameter, P = dispensing pressure (bar) and V = printing velocity (mm/s).

	Ø = 0.20 mm	**Ø = 0.25 mm**	**Ø = 0.41 mm**
P7.5_CaCl2_0.5	**P** (bar) = 2	**P** (bar) = 1.5	**P** (bar) = 1
	V (mm/s) = 7.5	**V** (mm/s) = 7.5	**V** (mm/s) = 7.5
P7.5_CaCl2_0.75	**P** (bar) = 2.5	**P** (bar) = 1.5	**P** (bar) = 1.0
	V (mm/s) = 7.5	**V** (mm/s) = 7.5	**V** (mm/s) = 10
P7.5_CaCl2_1	**P** (bar) = 2.5	**P** (bar) = 2	**P** (bar) = 1.0
	V (mm/s) = 7.5	**V** (mm/s) = 7.5	**V** (mm/s) = 7.5
P7.5_CaCl2_1.5	**P** (bar) = 2.5	**P** (bar) = 2	**P** (bar) = 1.5
	V (mm/s) = 5	**V** (mm/s) = 7.5	**V** (mm/s) = 7.5

For these assays, the formulations P7.5_CaCl2_1 and P7.5_CaCl2_1.5 presented in similar behavior, with optimal printing results at a pressure of 2 bar, a velocity of 7.5 mm/s, and using a 0.25 mm nozzle diameter. However, when it comes to printing a more complex construct (Figure 30), the formulation P7.5_CaCl2_1.5 led to clogging of the nozzle and lack of resolution on the final construct, this behavior is due to the higher viscosity granted by the higher concentration of $CaCl_2$. Due to this, the chosen

crosslinking formulation was P7.5_CaCl2_1, as it led to a lesser clogging of the nozzle due to the lower crosslinking concentration (Figure 30).

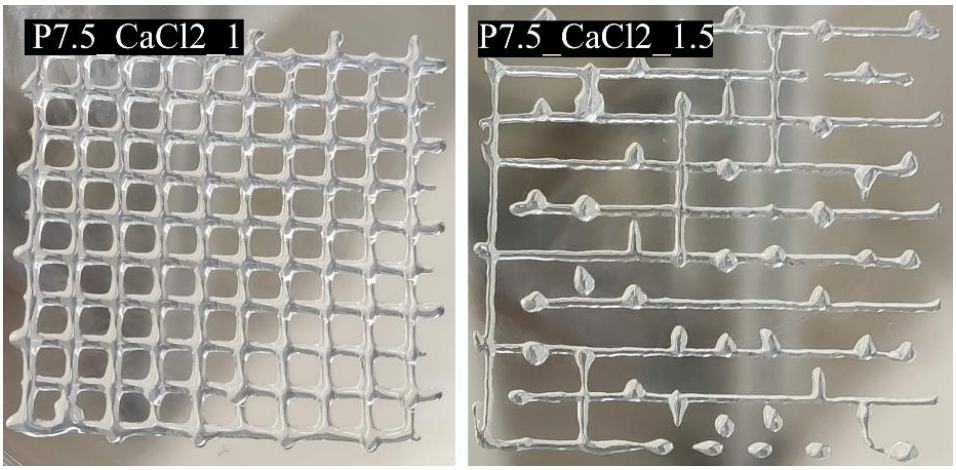

Figure 30 – Printing results of P7.5_CaCl2_1 (left) and P7.5_CaCl2_1.5 (right), using a 0.25 mm nozzle diameter.The formulation P7.5_CaCl2_1.5 presented more clogging, which resulted in a non-continuous ink deposition.

Considering this, the following printing parameters, pressure of 2 bar, velocity of 7.5 mm/s, and a nozzle diameter of 0.25 mm were chosen due to the balance between, printing resolution, velocity, and potential higher cell viability. After optimizing these parameters, the printability of the pectin-NFC inks was tested, and P7.5/NFC1_CaCl2_1 and P7.5/NFC10_CaCl2_1 formulations were printed, using different spacing between lines (1.5 mm or 2.5 mm), layer height (320 μm or 100 μm), layers printed (4, 6 or 8), or needle offset (0.75 mm or 0.50 mm). Figure 31 shows the printing results of the different constructs of P7.5/NFC1_CaCl2_1 and P7.5/NFC10_CaCl2_1 formulations, immediately after printing and after 24 h in a $CaCl_2$ bath.

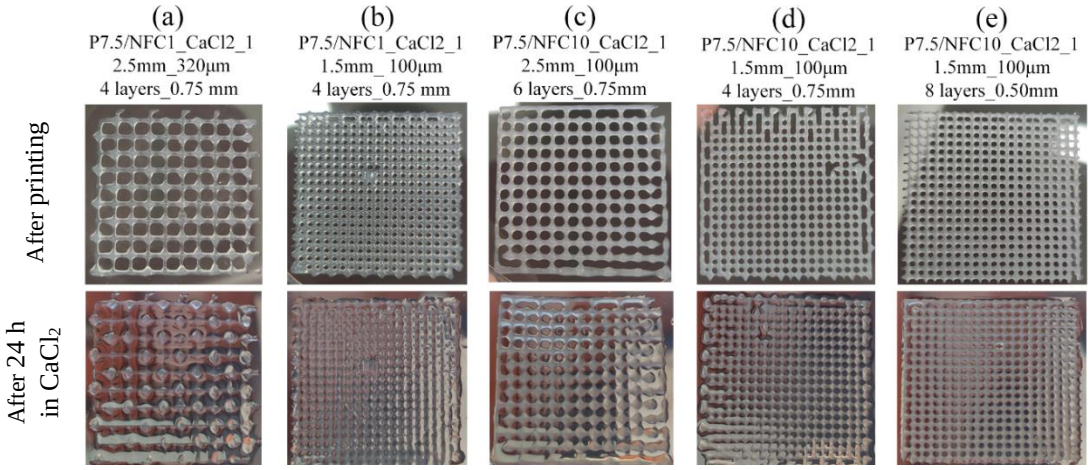

Figure 31 – Printed Pectin-NFC inks/hydrogels using different spacing between lines (1.5 mm or 2.5 mm), layer height (320 µm or 100 µm), layers printed (4,6 or 8) and needle offset (0.75 mm or 0.50 mm). The top-side images demonstrate the inks immediately after printing, while the bottom-side images represent the fully-crosslinked hydrogels obtained after a 24 h crosslinking step. (Ex: Sample – spacing_between_ lines – height – layers – needle offset).

The main factors to consider in order to obtain a high resolution and precision mesh, are spacing between lines and height between layers. Due to this the samples with spacing of 2.5 mm and/or height of 320 µm (sample (a) and (c)) were quickly discarded. According to the final constructs obtained (Figure 31), the most precise was sample (e) P7.5/NFC10_CaCl2_1, with 1.5 mm between lines, a layer height of 100 µm, and a needle offset of 0.50 mm. The needle offset was changed from 0.75 mm to 0.50 mm due to the gaps created by a distant needle, by reducing the space between the needle and the printing platform, the ink could connect to the other layers or platform, resulting in a continuous print of up to 8 layers. After the complete crosslinking bath of $CaCl_2$ 3% (m/v), the structure (e) composed of P7.5/NFC10_CaCl2_1, with 1.5 mm between lines, a layer height of 100 µm, and a needle offset of 0.50 mm, presented high shape fidelity, as it remained with precise pores and stiff matrix even after crosslinking. Taking these results into account, these would be the optimal 3D – printing settings for the chosen P7.5/NFC10_CaCl2_1 ink.

4. Conclusion

The objective of this work was the development of pectin-nanocellulose based bioinks for applications in 3D-bioprinting. A set of inks were prepared by mixing a citrus peel pectin solution with NFC in different amounts, followed by a pre-crosslinking step with the addition of a small amount of a $CaCl_2$ solution. All the pectin-NFC formulations presented shear thinning properties which are highly desirable in 3D-bioprinting applications. The viscosity and shear stress of the inks increased with the content of NFC, but the most relevant effect is associated with the pre-crosslinking with $CaCl_2$. Afterwards, fully-crosslinked hydrogels were obtained, and their chemical structure, morphology, and cytotoxicity assessed. The hydrogels demonstrated a homogeneous rough surface and a porous structure, which are essential features for, cell adhesion and proliferation. Moreover, almost all pectin-NFC hydrogels showed non-citotoxicity towards HaCaT cells demonstrating their suitability for incorporation of cells envisioned for 3D-bioprinting. Regarding the optimization of the 3D printing conditions, a pressure of 2 bar, a velocity of 7.5 mm/s, and a nozzle diameter of 0.25 mm were selected as the best conditions for these samples. The sample with the most promising results was the P7.5/NFC10_CaCl2_1 ink which allowed for printing up to 8 layers with great resolution.

These results show the huge potential of pectin-nanocellulose inks for 3D-bioprinting of living tissue analogues. Nevertheless, there are still some important topics to be further studied:

- To print cell-laden pectin-NFC bioinks using the chosen parameters;
- To assess the post-printing cell viability;
- To investigate the cell proliferation and tissue formation in 3D-bioprinted constructs;
- To study the degradation of the hydrogel vs the formation of the new tissue;
- To determine how pectin impacts the toxicity of pectin - NFC hydrogels.

5. Bibliography

1. Transplant trends - UNOS. Available at: https://unos.org/data/transplant-trends/. (Accessed: 11th December 2019)

2. Ning, L. & Chen, X. A brief review of extrusion-based tissue scaffold bio-printing. *Biotechnol. J.* **12**, 1600671 (2017).

3. Herman, A. R. The history of skin grafts. *J. Drugs Dermatol.* **1**, 298–301 (2002).

4. Cao, Y., Vacanti, J. P., Paige, K. T., Upton, J. & Vacanti, C. A. Transplantation of chondrocytes utilizing a polymer-cell construct to produce tissue-engineered cartilage in the shape of a human ear. *Plast. Reconstr. Surg.* **100**, 297–304 (1997).

5. Berthiaume, F., Maguire, T. J. & Yarmush, M. L. Tissue Engineering and Regenerative Medicine: History, Progress, and Challenges. *Annu. Rev. Chem. Biomol. Eng.* **2**, 403–430 (2011).

6. Gopinathan, J. & Noh, I. Recent trends in bioinks for 3D printing. *Biomater. Res.* **22**, (2018).

7. Hospodiuk, M., Dey, M., Sosnoski, D. & Ozbolat, I. T. The bioink: A comprehensive review on bioprintable materials. *Biotechnol. Adv.* **35**, 217–239 (2017).

8. Ng, W. L., Chua, C. K. & Shen, Y.-F. Print Me An Organ! Why We Are Not There Yet. *Prog. Polym. Sci.* **97**, 101145 (2019).

9. Dababneh, A. B. & Ozbolat, I. T. Bioprinting Technology: A Current State-of-the-Art Review. *J. Manuf. Sci. Eng.* **136**, (2014).

10. Ng, W. L., Lee, J. M., Yeong, W. Y. & Win Naing, M. Microvalve-based bioprinting-process, bio-inks and applications. *Biomater. Sci.* **5**, 632–647 (2017).

11. Ovsianikov, A. *et al.* Laser photofabrication of cell-containing hydrogel

constructs. *Langmuir* **30**, 3787–3794 (2014).

12. Colosi, C., Costantini, M., Barbetta, A. & Dentini, M. Microfluidic bioprinting of heterogeneous 3d tissue constructs. in *Methods in Molecular Biology* **1612**, 369–380 (Humana Press Inc., 2017).

13. Murphy, S. V. & Atala, A. 3D bioprinting of tissues and organs. *Nat. Biotechnol.* **32**, 773–785 (2014).

14. Matai, I., Kaur, G., Seyedsalehi, A., McClinton, A. & Laurencin, C. T. Progress in 3D bioprinting technology for tissue/organ regenerative engineering. *Biomaterials* **226**, 119536 (2020).

15. Pati, F., Jang, J., Lee, J. W. & Cho, D. W. Extrusion bioprinting. in *Essentials of 3D Biofabrication and Translation* (eds. Atala, A. & Yoo, J. J. B. T.-E. of 3D B. and T.) 123–152 (Academic Press, 2015). doi:10.1016/B978-0-12-800972-7.00007-4

16. Marga, F. *et al.* Toward engineering functional organ modules by additive manufacturing. *Biofabrication* **4**, (2012).

17. Ozbolat, I. T. Extrusion-Based Bioprinting ∗ ∗With minor contributions by Monika Hospodiuk, The Pennsylvania State University. in *3D Bioprinting* 93–124 (Elsevier, 2017). doi:10.1016/b978-0-12-803010-3.00004-4

18. Gudapati, H., Dey, M. & Ozbolat, I. A comprehensive review on droplet-based bioprinting: Past, present and future. *Biomaterials* **102**, 20–42 (2016).

19. Demirci, U. Acoustic picoliter droplets for emerging applications in semiconductor industry and biotechnology. *J. Microelectromechanical Syst.* **15**, 957–966 (2006).

20. Workman, V. L., Tezera, L. B., Elkington, P. T. & Jayasinghe, S. N. Controlled generation of microspheres incorporating extracellular matrix fibrils for three-dimensional cell culture. *Adv. Funct. Mater.* **24**, 2648–2657 (2014).

21. Ozbolat, I. T. & Yu, Y. Bioprinting toward organ fabrication: Challenges and future trends. *IEEE Trans. Biomed. Eng.* **60**, 691–699 (2013).

22. Whyte, D. J., Rajkhowa, R., Allardyce, B. & Kouzani, A. Z. A review on the challenges of 3D printing of organic powders. *Bioprinting* **16**, e00057 (2019).

23. Gungor-Ozkerim, P. S., Inci, I., Zhang, Y. S., Khademhosseini, A. & Dokmeci, M. R. Bioinks for 3D bioprinting: An overview. *Biomater. Sci.* **6**, 915–946 (2018).

24. Lee, K. Y. & Mooney, D. J. Hydrogels for Tissue Engineering. *Chem. Rev.* **101**, 1869–1880 (2001).

25. Moldovan, N. I. Progress in scaffold-free bioprinting for cardiovascular medicine. *J. Cell. Mol. Med.* **22**, 2964–2969 (2018).

26. Weber, G. F., Bjerke, M. A. & DeSimone, D. W. Integrins and cadherins join forces to form adhesive networks. *J. Cell Sci.* **124**, 1183–1193 (2011).

27. Charest, J. L., Jennings, J. M., King, W. P., Kowalczyk, A. P. & García, A. J. Cadherin-mediated cell-cell contact regulates keratinocyte differentiation. *J. Invest. Dermatol.* **129**, 564–572 (2009).

28. Athanasiou, K. A., Eswaramoorthy, R., Hadidi, P. & Hu, J. C. Self-Organization and the Self-Assembling Process in Tissue Engineering. *Annu. Rev. Biomed. Eng.* **15**, 115–136 (2013).

29. Mironov, V. *et al.* Organ printing: tissue spheroids as building blocks. *Biomaterials* **30**, 2164–2174 (2009).

30. Kucukgul, C. *et al.* 3D bioprinting of biomimetic aortic vascular constructs with self-supporting cells. *Biotechnol. Bioeng.* **112**, 811–821 (2015).

31. Yu, Y. *et al.* Three-dimensional bioprinting using self-assembling scalable scaffold-free “tissue strands” as a new bioink. *Sci. Rep.* **6**, 28714 (2016).

32. Yin Yu & Ozbolat, I. T. Tissue strands as “bioink” for scale-up organ printing. in *2014 36th Annual International Conference of the IEEE Engineering in Medicine and Biology Society* 1428–1431 (IEEE, 2014). doi:10.1109/EMBC.2014.6943868

33. Ott, H. C. *et al.* Perfusion-decellularized matrix: Using nature’s platform to engineer a bioartificial heart. *Nat. Med.* **14**, 213–221 (2008).

34. Gilpin, A. & Yang, Y. Decellularization Strategies for Regenerative Medicine: From Processing Techniques to Applications. *Biomed Res. Int.* **2017**, 1–13 (2017).

35. Pati, F. *et al.* Printing three-dimensional tissue analogues with decellularized extracellular matrix bioink. *Nat. Commun.* **5**, 3935 (2014).

36. Skardal, A. *et al.* A hydrogel bioink toolkit for mimicking native tissue biochemical and mechanical properties in bioprinted tissue constructs. *Acta Biomater.* **25**, 24–34 (2015).

37. Pati, F. *et al.* Biomimetic 3D tissue printing for soft tissue regeneration. *Biomaterials* **62**, 164–175 (2015).

38. Sakai, S., Ueda, K., Gantumur, E., Taya, M. & Nakamura, M. Drop-On-Drop Multimaterial 3D Bioprinting Realized by Peroxidase-Mediated Cross-Linking. *Macromol. Rapid Commun.* **39**, 1700534 (2018).

39. Badylak, S. F. Xenogeneic extracellular matrix as a scaffold for tissue reconstruction. *Transpl. Immunol.* **12**, 367–377 (2004).

40. Ali, M. *et al.* A Photo-Crosslinkable Kidney ECM-Derived Bioink Accelerates Renal Tissue Formation. *Adv. Healthc. Mater.* **8**, 1800992 (2019).

41. Malda, J. & Frondoza, C. G. Microcarriers in the engineering of cartilage and bone. *Trends Biotechnol.* **24**, 299–304 (2006).

42. Goh, T. K. P. *et al.* Microcarrier culture for efficient expansion and osteogenic differentiation of human fetal mesenchymal stem cells. *Biores. Open Access* **2**,

84–97 (2013).

43. Tavassoli, H. *et al.* Large-scale production of stem cells utilizing microcarriers: A biomaterials engineering perspective from academic research to commercialized products. *Biomaterials* **181**, 333–346 (2018).

44. Levato, R. *et al.* Biofabrication of tissue constructs by 3D bioprinting of cell-laden microcarriers. *Biofabrication* **6**, 035020 (2014).

45. Tibbitt, M. W. & Anseth, K. S. Hydrogels as extracellular matrix mimics for 3D cell culture. *Biotechnol. Bioeng.* **103**, 655–663 (2009).

46. Hong, S. *et al.* 3D Printing of Highly Stretchable and Tough Hydrogels into Complex, Cellularized Structures. *Adv. Mater.* **27**, 4035–4040 (2015).

47. Ermis, M. *et al.* Hydrogels as a new platform to recapitulate the tumor microenvironment. in *Handbook of Nanomaterials for Cancer Theranostics* 463–494 (Elsevier Inc., 2018). doi:10.1016/B978-0-12-813339-2.00015-3

48. Fang, Y. *et al.* Binding behavior of calcium to polyuronates: Comparison of pectin with alginate. *Carbohydr. Polym.* **72**, 334–341 (2008).

49. Braccini, I. & Pérez, S. Molecular basis of Ca2+-induced gelation in alginates and pectins: The egg-box model revisited. *Biomacromolecules* **2**, 1089–1096 (2001).

50. Mironi-Harpaz, I., Wang, D. Y., Venkatraman, S. & Seliktar, D. Photopolymerization of cell-encapsulating hydrogels: Crosslinking efficiency versus cytotoxicity. *Acta Biomater.* **8**, 1838–1848 (2012).

51. Catoira, M. C., Fusaro, L., Di Francesco, D., Ramella, M. & Boccafoschi, F. Overview of natural hydrogels for regenerative medicine applications. *J. Mater. Sci. Mater. Med.* **30**, 115 (2019).

52. Müller, M., Becher, J., Schnabelrauch, M. & Zenobi-Wong, M. Nanostructured Pluronic hydrogels as bioinks for 3D bioprinting. *Biofabrication* **7**, 035006

(2015).

53. Skardal, A., Zhang, J. & Prestwich, G. D. Bioprinting vessel-like constructs using hyaluronan hydrogels crosslinked with tetrahedral polyethylene glycol tetracrylates. *Biomaterials* **31**, 6173–6181 (2010).

54. Gao, G. *et al.* Bioactive nanoparticles stimulate bone tissue formation in bioprinted three-dimensional scaffold and human mesenchymal stem cells. *Biotechnol. J.* **9**, 1304–1311 (2014).

55. Cunniffe, G. M. *et al.* Three-Dimensional Bioprinting of Polycaprolactone Reinforced Gene Activated Bioinks for Bone Tissue Engineering. *Tissue Eng. Part A* **23**, 891–900 (2017).

56. Zhang, W. *et al.* Fabrication and characterization of porous polycaprolactone scaffold via extrusion-based cryogenic 3D printing for tissue engineering. *Mater. Des.* **180**, 107946 (2019).

57. Xu, T. *et al.* Hybrid printing of mechanically and biologically improved constructs for cartilage tissue engineering applications. *Biofabrication* **5**, 015001 (2012).

58. Koti, P., Muselimyan, N., Mirdamadi, E., Asfour, H. & Sarvazyan, N. A. Use of GelMA for 3D printing of cardiac myocytes and fibroblasts. *J. 3D Print. Med.* **3**, 11–22 (2019).

59. Gu, Y., Zhang, W., Wang, H. & Lee, W. Y. Chitosan surface enhances the mobility, cytoplasm spreading, and phagocytosis of macrophages. *Colloids Surfaces B Biointerfaces* **117**, 42–50 (2014).

60. Duan, B., Hockaday, L. A., Kang, K. H. & Butcher, J. T. 3D Bioprinting of heterogeneous aortic valve conduits with alginate/gelatin hydrogels. *J. Biomed. Mater. Res. Part A* **101A**, 1255–1264 (2013).

61. Bertassoni, L. E. *et al.* Direct-write bioprinting of cell-laden methacrylated gelatin hydrogels. *Biofabrication* **6**, 024105 (2014).

62. Levato, R. *et al.* The bio in the ink: cartilage regeneration with bioprintable hydrogels and articular cartilage-derived progenitor cells. *Acta Biomater.* **61**, 41–53 (2017).

63. Koch, L. *et al.* Skin tissue generation by laser cell printing. *Biotechnol. Bioeng.* **109**, 1855–1863 (2012).

64. Michael, S. *et al.* Tissue Engineered Skin Substitutes Created by Laser-Assisted Bioprinting Form Skin-Like Structures in the Dorsal Skin Fold Chamber in Mice. *PLoS One* **8**, e57741 (2013).

65. Moon, S. *et al.* Layer by Layer Three-dimensional Tissue Epitaxy by Cell-Laden Hydrogel Droplets. *Tissue Eng. Part C Methods* **16**, 157–166 (2010).

66. Lee, H. J. *et al.* A New Approach for Fabricating Collagen/ECM-Based Bioinks Using Preosteoblasts and Human Adipose Stem Cells. *Adv. Healthc. Mater.* **4**, 1359–1368 (2015).

67. Zhang, Y., Yu, Y., Chen, H. & Ozbolat, I. T. Characterization of printable cellular micro-fluidic channels for tissue engineering. *Biofabrication* **5**, 025004 (2013).

68. Gao, Q., He, Y., Fu, J., Liu, A. & Ma, L. Coaxial nozzle-assisted 3D bioprinting with built-in microchannels for nutrients delivery. *Biomaterials* **61**, 203–215 (2015).

69. Gudapati, H., Yan, J., Huang, Y. & Chrisey, D. B. Alginate gelation-induced cell death during laser-assisted cell printing. *Biofabrication* **6**, 035022 (2014).

70. Xu, C., Chai, W., Huang, Y. & Markwald, R. R. Scaffold-free inkjet printing of three-dimensional zigzag cellular tubes. *Biotechnol. Bioeng.* **109**, 3152–3160 (2012).

71. Gruene, M. *et al.* Laser Printing of Three-Dimensional Multicellular Arrays for Studies of Cell–Cell and Cell–Environment Interactions. *Tissue Eng. Part C Methods* **17**, 973–982 (2011).

72. Diniz, I. M. A. *et al.* Pluronic F-127 hydrogel as a promising scaffold for encapsulation of dental-derived mesenchymal stem cells. *J. Mater. Sci. Mater. Med.* **26**, 153 (2015).

73. Leberfinger, A. N. *et al.* Bioprinting functional tissues. *Acta Biomater.* **95**, 32–49 (2019).

74. Das, S. & Basu, B. An Overview of Hydrogel-Based Bioinks for 3D Bioprinting of Soft Tissues. *J. Indian Inst. Sci.* **99**, 405–428 (2019).

75. Shim, J.-H., Kim, J. Y., Park, M., Park, J. & Cho, D.-W. Development of a hybrid scaffold with synthetic biomaterials and hydrogel using solid freeform fabrication technology. *Biofabrication* **3**, 034102 (2011).

76. Nuttelman, C. R. *et al.* Macromolecular monomers for the synthesis of hydrogel niches and their application in cell encapsulation and tissue engineering. *Prog. Polym. Sci.* **33**, 167–179 (2008).

77. Zargar, V., Asghari, M. & Dashti, A. A Review on Chitin and Chitosan Polymers: Structure, Chemistry, Solubility, Derivatives, and Applications. *ChemBioEng Rev.* **2**, 204–226 (2015).

78. Zhou, D. *et al.* Bioinks for jet-based bioprinting. *Bioprinting* **16**, e00060 (2019).

79. Duarte Campos, D. F. *et al.* The Stiffness and Structure of Three-Dimensional Printed Hydrogels Direct the Differentiation of Mesenchymal Stromal Cells Toward Adipogenic and Osteogenic Lineages. *Tissue Eng. Part A* **21**, 740–756 (2015).

80. Maranchi, J. P., Trexler, M. M., Guo, Q. & Elisseeff, J. H. Fibre-reinforced hydrogels with high optical transparency. *Int. Mater. Rev.* **59**, 264–296 (2014).

81. Visser, J. *et al.* Reinforcement of hydrogels using three-dimensionally printed microfibres. *Nat. Commun.* **6**, 6933 (2015).

82. Klemm, D., Heublein, B., Fink, H.-P. & Bohn, A. Cellulose: Fascinating

Biopolymer and Sustainable Raw Material. *Angew. Chemie Int. Ed.* **44**, 3358–3393 (2005).

83. Portela, R., Leal, C. R., Almeida, P. L. & Sobral, R. G. Bacterial cellulose: a versatile biopolymer for wound dressing applications. *Microb. Biotechnol.* **12**, 586–610 (2019).

84. Hickey, R. J. & Pelling, A. E. Cellulose Biomaterials for Tissue Engineering. *Front. Bioeng. Biotechnol.* **7**, 45 (2019).

85. Rees, A. *et al.* 3D Bioprinting of Carboxymethylated-Periodate Oxidized Nanocellulose Constructs for Wound Dressing Applications. *Biomed Res. Int.* **2015**, 1–7 (2015).

86. Markstedt, K. *et al.* 3D Bioprinting Human Chondrocytes with Nanocellulose–Alginate Bioink for Cartilage Tissue Engineering Applications. *Biomacromolecules* **16**, 1489–1496 (2015).

87. Pereira, R. F., Sousa, A., Barrias, C. C., Bártolo, P. J. & Granja, P. L. A single-component hydrogel bioink for bioprinting of bioengineered 3D constructs for dermal tissue engineering. *Mater. Horizons* **5**, 1100–1111 (2018).

88. Munarin, F., Tanzi, M. C. & Petrini, P. Advances in biomedical applications of pectin gels. *Int. J. Biol. Macromol.* **51**, 681–689 (2012).

89. Cernencu, A. I. *et al.* Bioinspired 3D printable pectin-nanocellulose ink formulations. *Carbohydr. Polym.* **220**, 12–21 (2019).

90. Martoïa, F., Dumont, P. J. J., Orgéas, L., Belgacem, M. N. & Putaux, J.-L. Micro-mechanics of electrostatically stabilized suspensions of cellulose nanofibrils under steady state shear flow. *Soft Matter* **12**, 1721–1735 (2016).

91. Bjrn, A., La Monja, P. S. de, Karlsson, A., Ejlertsson, J. & H., B. Rheological Characterization. in *Biogas* (ed. Monja, P. S. de La) Ch. 3 (InTech, 2012). doi:10.5772/32596

92. King, R. P. Non-Newtonian slurries. in *Introduction to Practical Fluid Flow* 117–157 (Butterworth-Heinemann, 2002). doi:10.1016/b978-075064885-1/50005-3

93. Kar, F. & Arslan, N. Effect of temperature and concentration on viscosity of orange peel pectin solutions and intrinsic viscosity–molecular weight relationship. *Carbohydr. Polym.* **40**, 277–284 (1999).

94. Paxton, N. *et al.* Proposal to assess printability of bioinks for extrusion-based bioprinting and evaluation of rheological properties governing bioprintability. *Biofabrication* **9**, 044107 (2017).

95. Hölzl, K. *et al.* Bioink properties before, during and after 3D bioprinting. *Biofabrication* **8**, 032002 (2016).

96. ESDU. *Non-Newtonian fluids: Guide to classification and characteristics. 97034*. (ESDU International PLC, 2004).

97. Hazur, J. *et al.* Improving alginate printability for biofabrication: establishment of a universal and homogeneous pre-crosslinking technique. *Biofabrication* **12**, 045004 (2020).

98. Blaeser, A. *et al.* Controlling Shear Stress in 3D Bioprinting is a Key Factor to Balance Printing Resolution and Stem Cell Integrity. *Adv. Healthc. Mater.* **5**, 326–333 (2016).

99. Bingham, E. C. *An investigation of the laws of plastic flow*. *Bulletin of the Bureau of Standards* **13**, (Washington, D.C. : U.S. Dept. of Commerce, Bureau of Standards : 1917, 1916).

100. Hospodarova, V., Singovszka, E. & Stevulova, N. Characterization of Cellulosic Fibers by FTIR Spectroscopy for Their Further Implementation to Building Materials. *Am. J. Anal. Chem.* **09**, 303–310 (2018).

101. Bellamy, L. J. *The Infrared Spectra of Complex Molecules*. *Journal of Chemical Education* **59**, (Springer Netherlands, 1980).

102. Rosa, M. F. *et al.* Cellulose nanowhiskers from coconut husk fibers: Effect of preparation conditions on their thermal and morphological behavior. *Carbohydr. Polym.* **81**, 83–92 (2010).

103. Fonseca, D. F. S. *et al.* Bacterial nanocellulose-hyaluronic acid microneedle patches for skin applications: In vitro and in vivo evaluation. *Mater. Sci. Eng. C* **118**, 111350 (2021).

104. Loh, Q. L. & Choong, C. Three-Dimensional Scaffolds for Tissue Engineering Applications: Role of Porosity and Pore Size. *Tissue Eng. Part B Rev.* **19**, 485–502 (2013).

105. Dranca, F. & Oroian, M. Ultrasound-Assisted Extraction of Pectin from Malus domestica 'Fălticeni' Apple Pomace. *Processes* **7**, 488 (2019).

106. ISO 10993-5:2009(E). *Biological Evaluation of Medical Devices—Part 5: Tests for In Vitro Cytotoxicity*. (2009).

107. Abdel-Massih, R., Hawach, V. & Boujaoude, M.-A. The Cytotoxic and Anti-proliferative Activity of High Molecular Weight Pectin and Modified Citrus Pectin. *Funct. Foods Heal. Dis.* **6**, 587 (2016).

108. Ajdary, R. *et al.* Acetylated Nanocellulose for Single-Component Bioinks and Cell Proliferation on 3D-Printed Scaffolds. *Biomacromolecules* **20**, 2770–2778 (2019).

109. Nair, K. *et al.* Characterization of cell viability during bioprinting processes. *Biotechnol. J.* **4**, 1168–1177 (2009).

110. Chang, R., Nam, J. & Sun, W. Effects of Dispensing Pressure and Nozzle Diameter on Cell Survival from Solid Freeform Fabrication–Based Direct Cell Writing. *Tissue Eng. Part A* **14**, 41–48 (2008).

111. Adhikari, J. *et al.* Effects of Processing Parameters of 3D Bioprinting on the Cellular Activity of Bioinks. *Macromol. Biosci.* **21**, 2000179 (2021).